Detection of expansive soils using remote sensing in Brits, North-West Province, South Africa

by

Nondumiso Jacqueline Dlamini

Submitted in partial fulfillment of the requirements for the
degree Master of Science (MSc) in Geography

in the Faculty of Natural & Agricultural Sciences

University of Pretoria ©

Supervisor: Dr O.J. Botai (UP)

Co-supervisor: Dr. M.A. Cho (CSIR)

April 2015

UNIVERSITEIT VAN PRETORIA
UNIVERSITY OF PRETORIA
YUNIBESITHI YA PRETORIA

Abstract

Expansive soils generally pose a significant geological hazard, which causes damage to civil infrastructure that could amount to billions of rand every year. Traditionally, expansive soils have been mapped and characterized using methods such as X-ray Diffraction (XRD) and standard engineering tests such as Atterberg limits. These traditional methods have proven to be time consuming, labour intense and expensive. Remote sensing has shown potential as a faster, cheaper non-laborious complementary tool that will support traditional methods of mapping expansive soils and geotechnical investigation. Notwithstanding the significance of remote sensing techniques and their applications in mapping expansive soils, research in this field is at its infancy in South Africa. The purpose of this study is to map expansive soils by use of multi-disciplinary techniques i.e., identify expansive soils using field observations, laboratory techniques and multispectral remote sensing. Soil samples (53) were collected from Brits in the North West Province. The soil samples were classified into swelling and non-swelling soils using laboratory-based techniques. In this regard, a) X-ray Diffraction (XRD) was used for mineralogical identification and classification, b) Atterberg limits tests were used to estimate swell potential of soils and support soil classification, and c) spectroscopic measurements of soil were acquired under laboratory conditions using a hand-held Analytical Spectral Device (ASD). Results show that expansive soils are dominant in the study area, with smectite being the most dominant clay mineral. Analysis of malleability demonstrated that soil plasticity varies from non-plastic to very high plasticity. Soils with medium to very high plasticity are in majority. Using an ASD that collects data in the 350-2500nm wavelength region, swelling soils were identifiable in the SWIR region of the electromagnetic spectrum. Mean reflectance spectra of swelling and non-swelling soils were used to map these soils on ASTER imagery, using SAM classifier. In spite of the difficulties of acquiring enough ASTER images, mapping of expansive soils using remotely sensed imagery demonstrated potential of studying the distribution of expansive soils as well aid in geotechnical investigations with inherent spatial-temporal resolution merits.

Declaration

I, Nondumiso J Dlamini declare that the dissertation, which I hereby submit for the degree (Master of Science) MSc in Geoinformatics at the University of Pretoria, is my own work and has not previously been submitted by me for a degree at this or any other tertiary institution.

SIGNATURE: ……..

DATE: …….…….

Acknowledgements

I would like to extend my gratitude and express sincere thanks to

- the Department of Science and Technology for funding this project, as part of the Earth Observation and Geohazard Assessment project.
- the CGS, CSIR and ARC for the services offered.
- Dr Jeanine Engelbrecht, Dr Chiedza Musekiwa and Dr M. Cloete for giving me the opportunity to do this project.
- Dr Moses Cho and Dr J. Botai thank you for your supervision and guidance.
- Maria Atanasova, Eric Economon, Dr Souleymane Diop, Daniel Sebake, Tshepo Ratsane, Siphindiwe Noruka, Charmaine Thomas and Lucky Semelani I appreciate the time you gave into the project and your assistance.
- Ingrid Booysen for technical editing
- especially my son Qhayiya for allowing me the time to finish this project. Ngiyabonga.

Table of Contents

List of Figures

List of Tables

Abbreviations

AASTHO	American state of Highway and Transportation Officials
ARC	Agricultural Research Council
ASD	Analytical Spectral Device
ACORN	Atmospheric CORrection Now
ASTM	American Society of Testing Materials
ASTER	Advanced Spaceborne Thermal Emission and Reflection Radiometer
AVIRIS	Airborne Visible/Infrared Imaging Spectrometer
CI	Carbonate Index
CEC	Cation Exchange Capacity
CGS	Council for Geoscience
CSIR	Council for Scientific and Industrial Research
DTA	Differential Thermal Analysis
DN	Digital Numbers
ENVI	Environment for Visualizing Images
GPS	Global Positioning System
HyMap	Hyperspectral Mapper
ICDD	International Centre for Diffraction Data
I/S	Illite/Smectite
LL	Liquid Limit
MI	Mafic Index
MODTRAN	MODerate resolution atmospheric TRANsmission
NDVI	Normalised Difference Vegetation Index
NIR	Near Infrared
PL	Plastic Limit
PI	Plastic Index
QI	Quartz Index
RGB	Red Green Blue
RIR	Reference Intensity Ratio
RM	Reference Material
ROI	Regions Of Interest
SWIR	Short Wave Infrared
SL	Shrinkage Limit
TEM	Transmission Electron Micrograph

TIR	Thermal Infrared
UCC	Unit Conversion Coefficient
USGS	United States Geological Survey
VNIR	Visible to Near Infrared
Wt%	Weight percentage
XRD	X-Ray Diffraction
XRF	X-Ray Fluorescence

Chapter 1. The problem of expansive soils

1.1. Introduction

Expansive soils are highly plastic soils that undergo volumetric changes due to variations in moisture content in the soil (Horn and Strydom, 1998). They swell when they are wet and shrink upon drying leaving large voids (desiccation cracks) in the soil. Consequently, the soils are unstable and hazardous. Swelling is a result of chemical attraction of water molecules into the sheet structure of clay minerals in the soil (Das, 2002). Expansive soils are also referred to as swelling, active, shrinkable or heaving clay. In South Africa, they are mostly referred to as swelling clay (Diop et al., 2011). In this report, expansive and swelling soils will be used interchangeably.

Expansive soils pose a significant geological hazard that causes civil infrastructure damage. Globally, the damage is estimated to cost billions of dollars per year (Nelson and Miller, 1992; Gourley et al., 1993; Yitagesu, 2006). The presence of expansive soils and associated problems have been reported in five continents (Chen, 1988) and in more than sixty countries (Al-Rawas, 1999; Shi et al., 2002). Regions that experience significant moisture changes especially in semi-arid areas are highly affected by swell-shrink consequences of expansive soils. Lightweight buildings, shallow foundations, roads, and pavements are mostly affected by swell-shrink cycles of expansive soils, causing cracking, distortion and misalignment of doors and windows. Slope instability, gully formation, and difficult ground operations are further problems associated with expansive soils (Yitagesu, 2006).

In South Africa, the Department of Public Works (DPW) classifies expansive soils as problematic soils, with major cost and safety implications on civil infrastructure (DPW, 2011). An estimated R2 billion was used in 2008/9 to maintain South African government funded low cost housing due to damages caused by expansive soils (Diop et al., 2011). Their presence generally results in expensive design, higher construction cost, and expensive maintenance and affects the overall performance of a structure. Yitagesu et al., (2009) argues that expansive soils should be identified together with their expansion potential during geotechnical site investigation. This would ensure proper site selection, environmental compatibility and economically feasible designing and construction. Goetz et al., (2001) stated that in developing countries, construction activities usually proceed without proper or

satisfactory geotechnical investigations conducted on a site due to expensive and time-consuming testing methods.

Traditionally, expansive soils have been identified by field observations and by laboratory mineral identification methods such as X-ray Diffraction (XRD). Swelling potential of soil has previously been determined using direct and indirect engineering methods such as swelling pressure testing and Atterberg limits. However, these methods tend to be expensive and are not commonly used in soil mechanics laboratories but are important in research laboratories (Chen, 1988). High cost implications of sampling and laboratory analysis may lead to a very limited number of samples being collected at any site. This may lead to a poor representation of a site and the presence of expansive soils may be overlooked. The above mentioned factors have motivated for the exploration of methods that are faster and cheaper in identifying (mapping) and characterizing expansive soils (Goetz et al., 2001; Kariuki et al., 2003).

Remote sensing has shown potential as a faster, cheaper non-laborious complementary technique that will support traditional methods of mapping and geotechnical investigations (Yitagesu et al., 2009). As a tool, it is based on acquisition of quantitative spectral data of reflected and emitted electromagnetic radiation from the earth surface (Lillesand et al., 2008). Remote sensing datasets available for mapping and geotechnical investigation include reflectance spectroscopy (laboratory, field, or imaging) and satellite imagery. Reflectance spectroscopy is hyperspectral, meaning it acquires data in many very narrow contiguous spectral bands. While, multispectral imagery has fewer, broad wavebands, for instance Advanced Spaceborne Thermal Emission and Reflection Radiometer (ASTER) (Lillesand et al., 2008). Reflectance spectroscopy (laboratory and field) has potential as a rapid and non-destructive method of mineral identification (Kariuki et al., 2003). Satellite images can provide a large-area or synoptic coverage that allows for examination of an area on a regional scale or in single scene to get finer detail (Lillesand et al., 2008). Satellite images are particularly useful in remote areas because, data can be acquired without physically entering the place.

There is a growing interest in the use of remote sensing as a mapping tool. Its applications include terrestrial mapping and monitoring, land use planning and mineral exploration. Ninomiya (2005) used ASTER for detecting lithology. Qui et al. (2006) demonstrated the

effectiveness of ASTER in detecting lithological units**.** Kariuki et al. (2002) reported on the use of spectroscopy as a tool to study swelling soils. Yitagesu (2006) used spectroscopy to derive engineering parameters of expansive soils. The purpose of this study was to identify expansive soils using field observations, laboratory, and remote sensing techniques. It formed part of a bigger project that aimed to create an inventory and database of known geological hazards in South Africa.

1.2. Problem statement

There is no doubt that expansive soils are a major geological hazard in South Africa. The effect of expansive soils manifest in shallow foundations, roads, pavements and lightweight buildings, which are common to the majority of poor population. In particular, expansive soils cause cracking, distortion and misalignment of doors and windows. Furthermore, slope instability and gully formation are some of the problems associated with expansive soils. Notwithstanding the obvious problems related to expansive soils, coordinated studies on the mineralogy and geotechnical aspects of expensive soils are limited. This problem is exacerbated by the fact that traditional methods of identifying expansive soils and geotechnical investigation are time-consuming, labour intensive and expensive. This research will contribute towards demonstrating the capability of remote sensing techniques in the identification of expansive soils and geotechnical investigations. In the event that expansive soils can be successfully identified and classified using remote sensing, it will establish a faster, cheaper non-laborious complementary tool that support traditional methods of mapping expansive soils and geotechnical investigations.

1.3. Aim and objectives

The main purpose of this study is to identify expansive soils using field observations, laboratory, and remote sensing techniques. To achieve the general aim of the proposed study, the following specific objectives were set:

- To identify expansive soils in the study area using XRD and Visible-Near infrared spectroscopy.
- To classify soils into expansive and non-expansive soils based on XRD and Atterberg limits data.

- To map expansive and non-expansive soils using ASTER imagery.

Chapter 2. Literature Review

This chapter discusses expansive soils and clay minerals, their relationships, characteristics and their occurrences in South Africa. It further discusses traditional methods of identifying and characterization of expansive soils and clay minerals. Moreover, the potential role of remote sensing in identifying expansive soils and clay minerals, using laboratory reflectance spectroscopy and multispectral imagery (ASTER), is presented.

2.1. Expansive soils and clay minerals

Expansive soils are highly plastic soils that undergo volumetric changes due to variations in moisture content in the soil (Horn and Strydom, 1998). Expansive soils owe their characteristics to the type and the amount of clay minerals present in the soil. Clay mineralogy is the most important factor that controls the properties of expansive soils (Mitchell, 1993; Chen, 1988; Gourley et al., 1993). Clay fraction and specific surface area of clays may increase expansion potential of the soil through increased area for water affinity (Carter and Bentley, 1991; Chen, 1988). However, clay mineralogy determines the way in which soil particles stick together and the extent of volumetric (swell-shrink) changes due to water.

Clay minerals are hydrous phyllosilicates (sheet silicates) almost all made up of repeating layers of tetrahedral silicate and octahedral hydroxide sheets (Deer et al., 1992; Horn and Strydom, 1998; Nesse, 2000). The arrangements of these sheets give rise to two types of clay mineral structures, namely 1:1 and 2:1 structure. Clays with a 1:1 structure have one tetrahedral sheet and one octahedral sheet; the kaolinite group is an example of a 1:1 structure. Clay minerals such as illite, vermiculite, and smectite are examples of a 2:1 structure. Clays with 2:1 structure have an octahedral sheet packed in between two tetrahedral sheets (Deer et al., 1992; Nesse, 2000). The sheet structures of clay minerals influence physicochemical properties of soil; such properties include cation exchange capacity, plasticity, workability, green strength, and refractoriness (Horn and Strydom, 1998). A table that shows classification of the phyllosilicates and related clay minerals is presented in Appendix A (modified after Horn and Strydom, 1998).

Clay minerals are origin dependent and can vary from one geographic location to another (Velde, 1992). Clay minerals occur as fine-grained (<0.0002mm) crystalline, amorphous patty or fibrous particles in sediments, sedimentary and altered rocks, and soils (Deer et al., 1992). They occur in sedimentary rock units such as shale, mudstone, and siltstone and in altered rocks such as slate and phyllite. In soils, clay minerals may occur as residual or as transported materials. Residual soils prone to expansiveness are generally a product of chemical weathering of basic igneous rocks and argillaceous sedimentary rocks (Horn and Strydom, 1998). Argillaceous rock units of the Karoo Supergroup and Uitenhage cretaceous marine formations are important sources of expansive soils in Southern Africa (Williams et al., 1985). The Karoo Supergroup is a parent material to the shale and mudrock of Ecca and Beaufort Group, and the shale, mudrock, tillite and varvites of the Dwyka Formation. Important basic igneous rocks include dolerites of the Karoo Supergroup, norites of the Bushveld Igneous Complex, andesites or dolerites in the Pretoria Group of Transvaal Supergroup and the andesitic lavas of the Ventersdorp Supergroup (Williams et al., 1985). Occurrences of transported expansive soils in South Africa include lacustrine deposits, colluvium and alluvium deposit as well as gulleywash deposits. Examples include Vereeniging clay (alluvium deposit) and the black clay in the Pretoria Moot area gulleywash deposit (Williams et al., 1985). The regional distribution of swell clay occurrence in South Africa is shown in Figure 1.

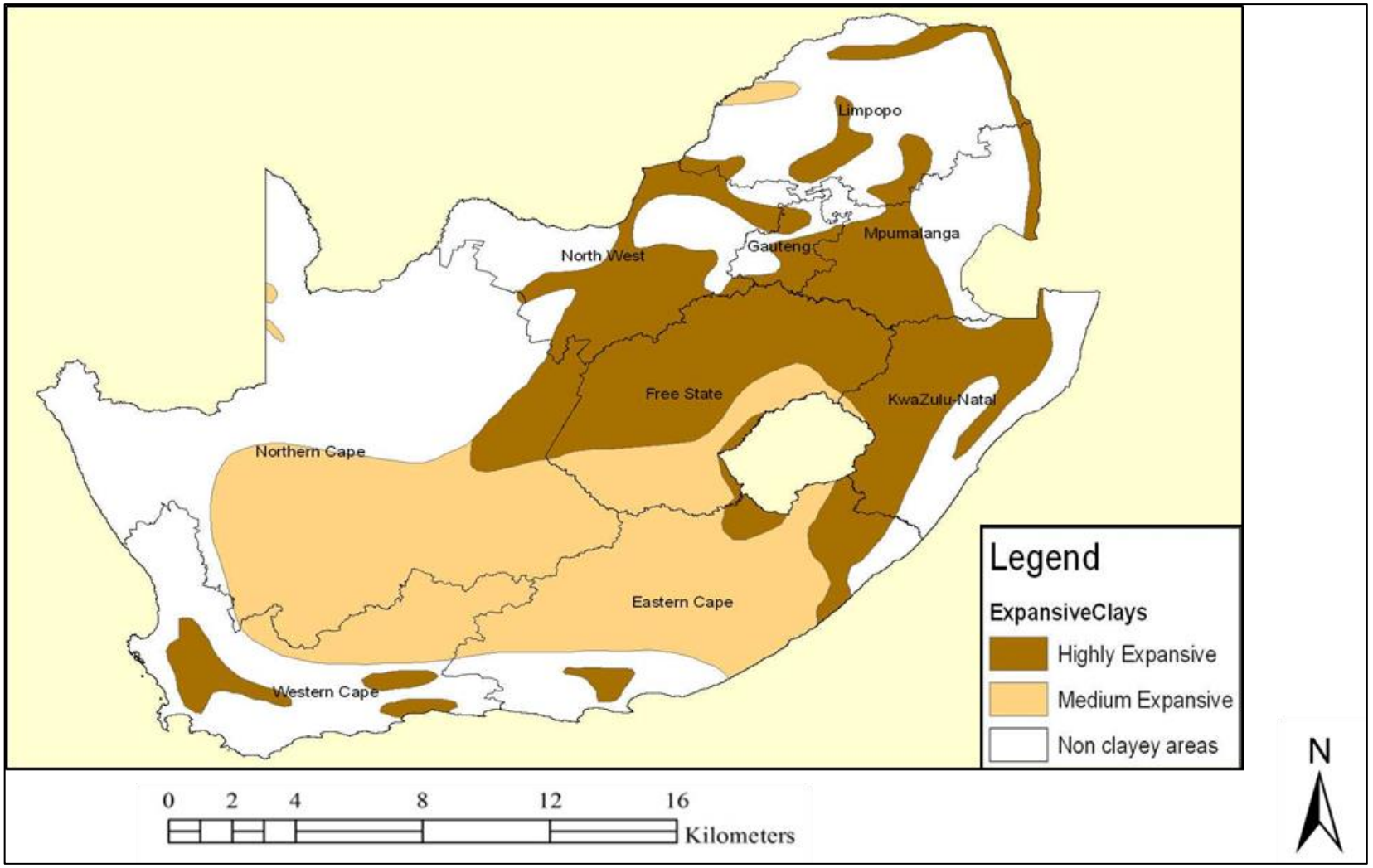

Figure 1: Map showing regional distribution of swell clay occurrence in South Africa. DPW (2007) document.

Some of the most dominant clay minerals include kaolinite, illite, montmorillonite (smectite) and interstratification (mixed layer clays). Kaolinite, $Al_4[Si_2O_{10}](OH)_8$ is a commonly occurring clay mineral in soils. According to Deer et al., (1992), Kaolinite is the most important member of the kaolinite group, which also include dickite, nacrite, halloysite, allophane and imogolite. It generally occurs as a primary residual deposit formed by weathering of aluminium silicate minerals like feldspars and muscovite in acidic rocks or as a product of low-temperature hydrothermal alteration of these minerals. It is found in subtropical to tropical environments with good drainage systems and high leaching rates of soluble elements such as potassium, sodium that enrich the residue in aluminuim and silicon (Horn and Strydom, 1998). Kaolinites commonly occur in association with quartz and feldspars, goethite, or amorphous iron oxides, anatase and rutile. They are usually white, sometimes red, blue or a brown shade from impurities; iron oxide may colour it pink-orange-red. They are soft (Mohs scale 2-2.5) with a specific area of $15m^2/g$ and a low cation exchange capacity ranging from 10µeq./g up to 100μeq./g (Deer et al., 1992). As mentioned before kaolinite has a 1:1 structure, the layers are held together by hydrogen bonds (Das, 2002). Kaolinites have no swell/shrink capacity (they are not expandable).

Illite $(K,H_3O)(Al,Mg,Fe)_2(Si,Al)_4O_{10}[(OH)_2,(H_2O)]$ also known as “mica-like” clay mineral, includes hydrous micas, phengite, brammalite, celadonite and glauconite in its group. It is soft (Moh’s scale1-2), with a specific area of $80m^2/g$ and a moderate cation exchange capacity between 100µeq./g and 400µeq./g. It has a 2:1 structure and has no shrink-swell capacity (Nesse, 2000 and Deer et al., 1992). It is grey-white to silvery-white, greenish-grey coloured. It is mainly formed by low-grade metamorphic process such as burial metamorphism of smectite and may be formed from alteration of minerals like muscovite, kaolinite and feldspars (Deer et al., 1992). Illite is found in low-grade metamorphic rocks, argillaceous sedimentary rocks, sediments, and soils. It is the main constituents of shales. In natural environments, it is common to find illite intermixed with smectite (Deer et al., 1992).

Smectite is a group of minerals that is comprised of montmorillonite, nontronite and saponite. Montmorillonite [$(Na,Ca)_{0.33}(Al,Mg)_2(Si_4O_{10})(OH)_2 \cdot nH_2O$] is the most commonly occurring smectite mineral (Deer et al., 1992). Smectite has a 2:1 structure, which allows moisture into its structure and has a high shrink-swell capacity. It has a high specific area 800m^2/ g and a high cation exchange capacity ranging between 800µeq./g to 1500µeq./g. It is soft (Mohs scale1-2) and may appear white, pale pink, blue, yellow, red, or green in colour. It is a weathering product of volcanic ash, bentonite and silicate minerals such as olivines, amphiboles and feldspars. It is formed in areas where silica is abundant with low rainfall or blocked drainage, conditions that do not promote chemical weathering. When chemical weathering is not promoted, soluble bases are not leached from the soil. This promotes the formation of smectite minerals (Chen, 1988). It often occurs intermixed with other clay minerals such as chlorite, muscovite, illite, cookeite, and kaolinite.

Interstratified or mixed-layer clay minerals refer to phyllosilicate structures where two or more layer-clays are intermixed at unit cell level (Nesse, 2000). Interstratified or mixed-layer clays may have varied structure (2:1 or 1:1) depending on the clay minerals making it up. The two minerals, mineral groups, or layer types present refer to them for example illite/smectite and chlorite/smectite. The two mixed-layer clays mentioned are the most commonly occurring mixed layer mineral series (Velde, 1992; Nesse, 2000). According to Deer et al., (1992) illite/smectite mixed-layer aggregate is the most abundant constituent of sedimentary rocks. It is common for mixed-layer clays to be expansive because of the general presence of smectite in them (Velde, 1992; Nesse, 2000). They occur in hydrothermal altered shales and in the chilled border zones of intrusive dolerite sheets.

2.2. Traditional methods of characterizing expansive soils and clay minerals

Identification of clay minerals is usually performed in a laboratory using different methods, which will be given in section 2.2.2. However, a good indication of their presence may be realized from field observation, and simple field-tests.

2.2.1. Field observation and simple field-tests

In the field, clayey soils are recognizable by their colour. They are often a black, dark grey, red, or mottled yellow-grey colour and on rare occasions, they may be light grey, brown, or white depending on their mineralogy (Deer et al., 1992). In addition, polygonal desiccation crack patterns in soils during dry seasons are indicative of the presence of clay minerals. The depth of desiccation cracks is associated with the amount of volume change that the soils had undergone upon drying. Simple field tests used for the identification of swelling soils include wetting and rolling soil into a tread of 3mm to 4mm thick and approximately 20mm long. If it rolls without breaking then it is expansive. In situ tests include free swell tests and soil suction measurements.

2.2.2. Laboratory identification of clay minerals

Traditional laboratory methods of identifying clay minerals include X-ray diffraction (XRD), electron microscope, microprobe, and cation exchange capacity method (Velde, 1992). These methods use different properties of clay minerals to identify them and give results in different formats. Electron microscopes such Scanning Electron Microscope (SEM) and Transmission Electron Microscopy (TEM) produce images of a sample in question. An electron microprobe is an X-ray fluorescence spectrometer with an electron microscope. Cation exchange capacity method measures the surface area and the charges of the surface area, these two properties are important for swelling properties of soil (Velde, 1992). XRD analysis was used for identification and semi-quantification of clay minerals in this study and will be discussed briefly below.

X-ray diffraction (XRD) analysis is a highly recommended and most relied on technique for clay mineral identification (Środoń, 2001). The XRD reveals information about the crystallographic structure, chemical composition, and physical properties of materials in question. Its applications are important in geology, environmental science, material science, engineering and biology (Środoń, 2001). It is particularly useful in the identification of unknown crystalline materials such as minerals and inorganic compounds. Other applications include characterization of crystalline materials and identification of materials that are too fine grained to be identified optically, for instance clays.

2.2.3. Estimating swell potential of soils

Direct and indirect measurements can be used to estimate swell potential of soils. Direct methods commonly used for swell determination include swelling pressure testing and free swell testing (Nelson and Miller, 1992; Yitagesu, 2006). Direct methods are executed in controlled laboratories to simulate natural environmental conditions. As a result, they are expensive, labour intensive and time consuming. However, these methods allow an opportunity to observe the behaviour of soil as it expands (Yitagesu, 2006).

Indirect techniques use index parameters such as cation exchange capacity and Atterberg limits to assess swelling potential of expansive soils. Atterberg limits are a basic measure of soil plasticity as a function of moisture variation. Soil plasticity is due to swelling clay minerals; soils without swelling clay minerals are non-plastic (Gourley et al., 1993, Mitchell, 1993, Thomas et al., 2000). Clayey soils behave differently at varying moisture contents; they may appear in a solid, semi-solid, plastic, and semi-liquid state. The boundaries between these four soil states are called Atterberg limits, namely shrinkage limit, plastic limit, liquid limit (Das, 2002). Shrinkage limit (SL) is a boundary between solid and semi-solid state of soil, it is a point where soil will no longer shrink due to drying. Plastic limit (PL) of soil is at a point where soil changes from semi-solid to plastic state due to increasing water content. Liquid limit (LL) of soil is at a point where soil changes from plastic to liquid

state as the water content increases (Das, 2002). Figure 2 is an illustration of the progression of clayey soil states from solid state to semi-liquid as the water content increases.

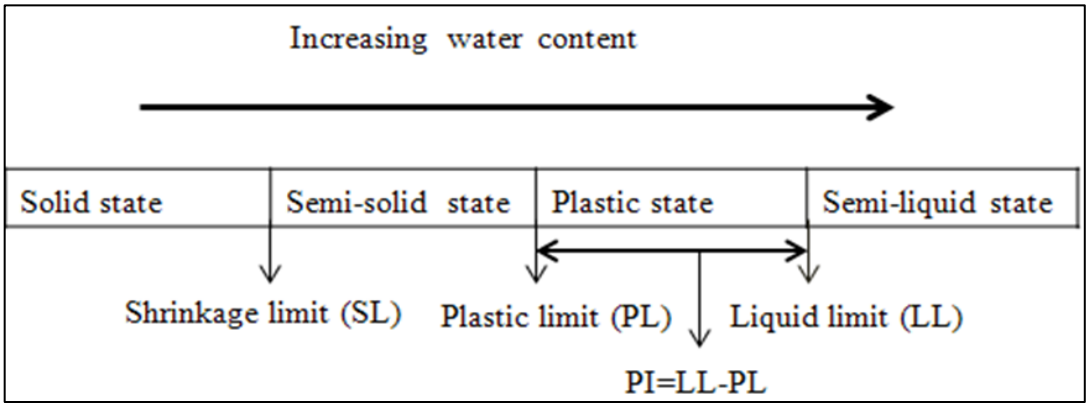

Figure 2: Schematic representation of soil states from solid to semi-liquid states at increasing water content and the respective Atterberg limits (Yitagesu, 2006).

Atterberg limits are widely used in engineering applications because of good correlations they show with engineering properties of soil (Das, 2002). Their use extends to construction quality specification and standards such as the American Society of Testing Materials (ASTM). Atterbergs limits were used in this study to estimate swell potential of each soil sample and subsequently classify it accordingly. Measured Atterberg limits are used to derive the Liquidity Index (LI) and Plasticity Index (PI). Liquidity index is a measure of relative consistency of plastic soils in a natural state; it is calculated by equation 1:

$$LI = \frac{W-PL}{LL-PL} \qquad (1)$$

Where, W is the natural water content

PL is the plastic limit of the soil

LL is the liquid limit of the soil

Plasticity index (PI) is a measure of soil's plasticity; it shows the range of water contents at which soils display plastic properties (Lambe and Whitman, 1979). It is calculated as a numerical difference between liquid limit and plastic limit,

$$PI = LL - PL \quad (2)$$

The plasticity index of any soil may vary from non-plastic, slightly plastic, low, medium, and high to very high plasticity and can therefore be used to classify soil accordingly. The plasticity index was used to classify soil samples in this study.

2.3. Remote sensing framework

Remote sensing is the science and art of obtaining information about an object, area or phenomenon through the analysis of data acquired by a device that is not in contact with the object, area or phenomenon under investigation (Jensen, 2005; Lillesand et al., 2008). This is done through acquisition of quantitative spectral data of reflected and emitted electromagnetic radiation from the earth surface (Lillesand et al., 2008). Various portions of the electromagnetic spectrum are important for mineral mapping including the visible and near infrared (VNIR), the short wave infrared (SWIR) and the thermal infrared (TIR) portions. Absorption features in the VNIR band are associated with cation bonds and electrical processes and are useful for mapping iron oxides and hydroxides such as hematite and goethite. The SWIR absorption features are related to vibration and stretching processes between water and cation molecules and are valuable in mapping dioctahedral and trioctahedral silicates including clay minerals and amphiboles. The TIR region is useful for mapping of framework silicates such as quartz and feldspars; the Si-O absorption feature in the TIR band supports this. Mineral mapping using remote sensing techniques is best when vegetation is at a minimum and soil and rocks are visible.

Research on mapping expansive soils by use of remote sensing techniques have been reported in the literature. Yitagesu et al. (2009) quantified engineering parameters of expansive soils such as Atterberg limits (LL, PL, and PI), free swell and cation

exchange capacity from their reflectance spectra. Results show that it is possible to identify and characterize expansive soils from their reflectance spectra. Additionally, strong correlations exist between engineering parameters of soil and reflectance spectra. Chabrillant et al. (2002) used hyperspectral images Airborne Visible/Infrared Imaging Spectrometer (AVIRIS) and the Hyperspectral Mapper HyMap for identifying and mapping expansive clay soils. The high spatial resolution provided by AVIRIS data produced good image endmembers in heterogeneous sites. However, compared to lower resolution HyMap data, AVIRIS did not produce more endmembers and did not identify more natural outcrops than the HyMap data. De Senna et al. (2008) used reflectance spectroscopy to characterize alluvium-derived ball-clay deposits used in the ceramic manufacturing industry in the São Simão. As reported in de Senna et al., 2008 three clay minerals (kaolinite, mica and smectite) were spectrally distinguishable and characterized successfully. Mineralogical indices such as Quartz Index (QI), Carbonate Index (CI), and Mafic Index (MI) were applied on ASTER-TIR data to identify quartzite, carbonate, and silicate rocks in selected areas of China and Australia. The rocks were distinguished effectively, and results corresponded with field observation as well as public geological maps of the area (Ninomiya et al., 2005). The remote sensing framework for this study is comprised of laboratory reflectance spectroscopy and ASTER imagery.

2.3.1. Laboratory reflectance spectroscopy

Reflectance spectroscopy has been used for many years to study earth materials such as soil and minerals (de Senna et al., 2008). It may be applied in the field or in laboratories. It is the study of the interaction between matter and radiated energy. Absorption of radiation at specific wavelengths generates reflectance spectra with characteristic absorption features of the matter, in this case soil (Jensen, 2007). Radiation is measured as a function of wavelength. Absorption feature properties such as shape, depth, area, width, symmetry, and position are dictated by physiochemical properties such as crystal and chemical structure of minerals in the soil (Chabrillant and Goetz, 2006). Absorption features hold information about the composition and mineralogy of soil and therefore, can be used for identifying and differentiating

minerals in the soil (Kariuki, 2003; Yitagesu, 2006; de Senna et al., 2008). Spectrometers are used to take spectroscopic measurements generally reported as reflectance, derived from Digital Numbers (DN) by the instrument automatically or may be calculated. Reflectance may be defined as a ratio of measured radiance from an object divided by radiance reflected by a near perfect reflector (Jensen, 2007). Figure 3 is an example of a soil reflectance spectrum showing absorption feature parameters in the visible and near infrared region of the electromagnetic spectrum.

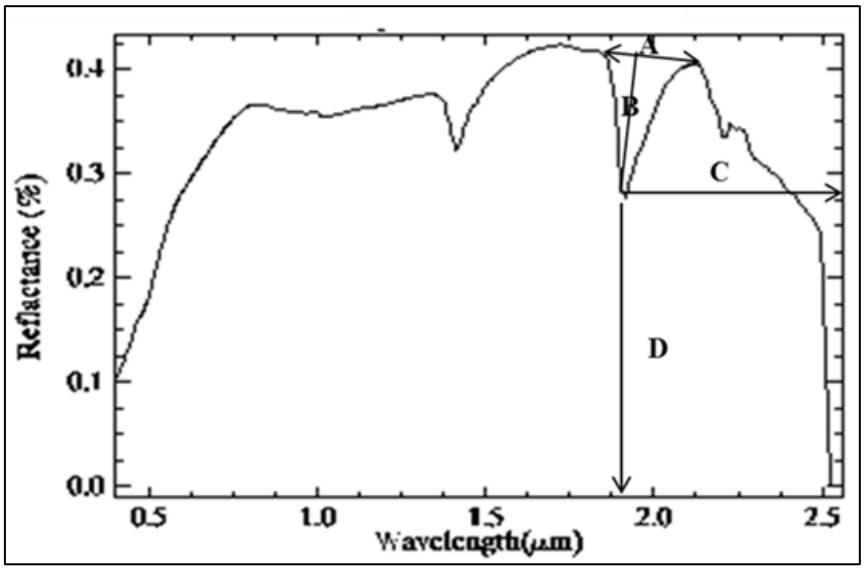

Figure 3: Soil spectrum showing absorption feature parameters (Yitagesu, 2006).

The following features, presented on Figure 3, can be used as diagnostic features:

A- Relative absorption width it is the distance between two shoulders of an absorption feature.

B - Relative absorption area is a sum of areas to the left and right of a line drawn in the centre of an absorption feature.

C - Relative absorption depth refers to the depth of an absorption feature relative to the hull

D - Position of an absorption feature, it is where minimum reflectance is observed. Absorption symmetry is a ratio of an area to the left and to the right of the centre of an absorption feature.

Spectral reflectance characteristics of soil are a function of factors such as; soil texture, soil moisture, organic matter content, iron oxide content, soil salinity, and surface roughness as they influence overall appearance of soil spectra (Van der Meer, 1999; Jensen, 2007). Soil texture and soil moisture content are highly influenced by clay mineral content and soil texture also influences organic matter content. The influence of soil texture, organic matter and soil moisture on soil spectral characteristics is briefly discussed below.

Soil texture is largely influenced by the amount and type of clay content. These in turn influence expansive properties of soil, soil structure and organic matter content of soil (Jensen, 2007). Soil particle size is an additional property of soil texture, with a decrease in the soil spectral reflectance being associated with an increasing particle size. This is due to smaller grains having more surface reflections and multiple scattering centres compared to larger particle sizes that have more internal path where photons may be absorbed and reflects less (Van der Meer et al., 2012). Another property related to soil texture is organic matter content. The presence of organic matter in soil reduces the overall brightness of spectra and may mask out absorption features. The amount of organic matter that may significantly influence soil spectra varies with different soils.

Soil waters influence soil spectra differently, which makes it possible to identify and distinguish between different soil waters. Identifiable soil waters include free pore waters, hygroscopic and hydration water and each of them have distinguishable features in the Short Wave Infrared (SWIR) region of the electromagnetic spectrum. Free pore waters and hygroscopic waters reduce the overall reflectance of soil (Bedidi et al., 1991), and, in excess quantities, may cause absorption features in 1400nm and 1900nm wavelength range to appear rounded. Hydration water have distinguishing features at shorter wavelengths, are narrower and may result in broadening of the 2200nm absorption band (Hauff, 2000). The 1900nm absorption band indicates hydration water and is therefore important as far as swelling potential is concerned (Chabrillant et al., 2002). High swelling potential is expected with a deeper and

broader 1900nm absorption band. The 1900nm absorption band can be used to discriminate between kaolinite and montmorrillonites or illite.

Expansive soils show absorption features in the SWIR region of the electromagnetic spectrum because of clay mineral's characteristic absorption features in this region (Goetz et al., 2001; Chabrillant and Goetz, 2006). Clay minerals are identifiable and can be discriminated using the SWIR region, the 1900nm-2500nm region is particularly important. In this region, the presence or the absence of hydroxyl and water molecules is important for differentiating clay minerals. These molecules produce vibrational processes that are responsible for energy absorption. Diagnostic absorption features due to hydroxyl radical and water molecules are manifested in the 1400nm and 1900nm bands respectively. The 1400nm absorption band is due to OH stretch overtone, while the 1900nm band is due to bound water and therefore may be indicative of swelling potential in clay minerals (Chabrillant and Goetz, 2006). All clay minerals show diagnostic absorption around 2200nm -2300nm due to Al-OH overtone combination (Chabrillant and Goetz, 2006).The position of the 2200nm band varies in the different clay minerals; the variation is due to the different ratios of Al, Fe and Mg cations (Crowley and Vergo, 1999). SWIR is sensitive to variations in the chemical and crystal structure of clay minerals.

Kaolinite group minerals show diagnostic doublet absorption bands at 1400nm and 2200nm. The 1400nm band is due to OH stretch overtone and 2200nm due to a combination of Al-OH bend and OH stretch (Hauff et al., 1991**).** These doublets absorption bands are characterized by a broad absorption with a sharper deeper band at slightly longer wavelength.

Illite and smectite (montmorillonite) have similar absorption bands. They both have a distinct 2200nm absorption band due to a combination of Al-OH and OH stretch, illite have additional bands at 2340nm and a poorly defined band at 2450nm (Chabrillant and Goetz, 2006). In smectite (montmorillonite), a shift of the 2200nm absorption band from 220nm 4 to 2214nm may be observed, after this absorption band a sharp

decrease in reflectance is observed. When illite and smectite occur as an illite/smectite interstratification, they show absorption features at 2200nm, 2340nm and have a higher reflectance at 2400nm than at 2200nm. The higher reflectance at 2400nm is an indication of the presence of illite, this becomes important if the 2340nm absorption band where illite content is not obvious (Chabrillant and Goetz, 2006). Table 1 show major absorption features of clay minerals (such as smectite, illite and kaolinite), absorption feature positions and responsible molecules like the hydroxyl and water molecules.

Table 1: Absorption feature positions of clay minerals and responsible molecules (Hauff, 2000).

Clay mineral	**Major feature position (nm)**	**Molecule**
Smectite/ Illite/ Kaolinite	1400	H_2O & OH
Smectite/ Illite	1900	H_2O
Kaolinite	2170	Al-OH
Smectite/ Illite/ Kaolinite	2200	Al-OH
Smectite (Notronite)	2290	Fe-OH
Smectite (Hectorite)	2300	Mg-OH/Mg-OH
Illite	2340	Fe-OH
Kaolinite	2384	Fe-OH

Reflectance spectra of montmorillonite (smectite), illite, kaolinite and I/S (illite/smectite interstratification) from the United States Geological Survey (USGS) spectral library (Clark et al., 1990) are displayed in Figure 4. The plots show diagnostic features at 1.4µm and the 1.9µm and between 2.0µm -2.5µm. The library plots show that clay minerals are distinguishable from each other. Plots of the same mineral may slightly differ amongst solid solutions of the same mineral.

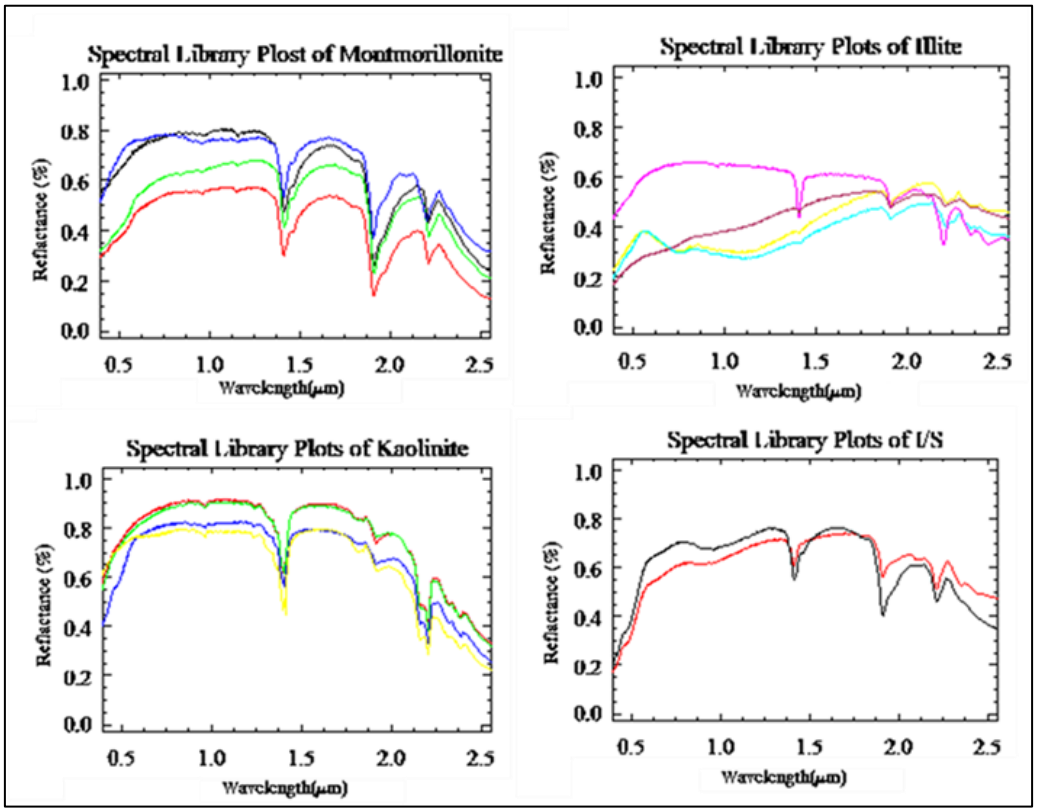

Figure 4: Reflectance spectra from the USGS spectral library, displaying montmorillonite (smectite), illite, kaolinite and I/S interstratification 0.5µm -2.5µm wavelength region (Clark et al., 1990).

2.3.2. ASTER Imagery

ASTER imagery was chosen for this study because it has sufficient spectral, spatial, and radiometric resolution for geological application (Ninomiya et al., 2005). ASTER's enhanced mineral mapping capabilities has seen its use grow (Van der Meer et al., 2012). However, ground truthing and appropriate thresholds setting are crucial when mapping with any imagery including ASTER. Imagery alone cannot, with complete confidence indicate the occurrence of a mineral nor can it quantify it, hence the results have to be validated. Table 2 show ASTER multispectral bands and their wavelength range, resolution and description of each band

Table 2: ASTER multispectral bands in the VNIR, SWIR and TIR of the electromagnetic spectrum (Rowan and Mars, 2003)

Band	Label	Wavelength(µm)	Resolution(m)	Description
B1	VNIR_Band1	0.520–0.600	15	Visible green/yellow
B2	VNIR_Band2	0.630–0.690	15	Visible red
B3	VNIR_Band3N	0.760–0.860	15	Near infrared
B4	VNIR_Band3B	0.760–0.860	15	
B5	SWIR_Band4	1.600–1.700	30	Short-wave infrared
B6	SWIR_Band5	2.145–2.185	30	
B7	SWIR_Band6	2.185–2.225	30	
B8	SWIR_Band7	2.235–2.285	30	
B9	SWIR_Band8	2.295–2.365	30	
B10	SWIR_Band9	2.360–2.430	30	
B11	TIR_Band10	8.125–8.475	90	Long-wave infrared or thermal IR
B12	TIR_Band11	8.475–8.825	90	
B13	TIR_Band12	8.925–9.275	90	
B14	TIR_Band13	10.250–10.950	90	
B15	TIR_Band14	10.950–11.650	90	

Mapping with imagery requires image processing before information can be extracted from an image. Image processing follows specific techniques or algorithms, depending on actual data usage. Processing techniques generally include the following steps pre-processing (includes image rectification and restoration), image enhancement and image classification (Lillesand et al., 2004). Pre-processing includes corrections for distortion due to the characteristics of the imaging system and imaging conditions. Such corrections include geometric, radiometric correction, crosstalk correction and atmospheric correction (Van der Meer et al., 2012). During processing, images may also be transformed to conform to a specific map projection system and may be geo-referenced to register an image to a precise map. Image enhancements are carried out in order to improve visual appearance of objects in an image, this aid with visual interpretation of an image. Techniques that may be employed for this purpose include grey level stretching to improve contrast and spatial filtering for enhancing edges (Lillesand et al., 2004). Image classification aims at automatically categorizing all pixels in an image into land cover classes or themes. Image classification involves

spatial, spectral and temporal pattern recognition. Image classifiers commonly used are supervised, unsupervised and hybrid classification (Lillesand et al., 2004).

Supervised classification technique (Spectral Angle Mapper) built in ENVI was used in this study. Spectral Angle Mapper (SAM) was chosen because it allows for direct comparison of image spectra, to laboratory spectra available in spectral libraries or measured spectra. Known spectra (measured spectra or from spectral libraries) and image spectra are both treated as vectors in an n -dimensional space, where n is the number of bands in the image. The spectral angle (in radians) between image spectra and reference spectra is calculated as a measure of similarity. The smallest angle represents the most similarity (Jensen, 2005).

Identification and mapping of soils swelling potential is a very important aspect of geotechnical site investigation. This step is important both financially and in terms of safety. However, due to cost implication, time and the nature of the work associated with identification and mapping of expansive soils and clay mineral. Construction activities usually proceed without proper or satisfactory geotechnical investigations. As mentioned before, this is common in developing countries. Remote sensing has potential to offer a faster, cheaper non-laborious complementary technique that will support traditional methods of mapping and geotechnical investigations. Hence, this research study proved important.

Chapter 3. Data collection and analysis

Data collection and analysis section presents the location of the study, why it was chosen and when the data was collected. It further presents laboratory methods used to analyse soil samples, such as XRD, Atterberg limits and spectroscopic measurements. Analyses of data comprise classification of soils into swelling and non-swelling soils. Classification validation was performed using statistical methods such as hierarchical clustering, factor analysis, discriminant analysis and bootstrapping approach. ASTER image analysis comprise pre-processing and classification of the image into soils into swelling and non-swelling soils, using Spectral Angle Mapper (SAM) supervised classification technique.

3.1. Study area

The study area (Figure 5) is located in the North West Province of South Africa near the town of Brits. It is a 728 km^2 area and falls within the following coordinates 27° 45'; 28° 00' E and 25° 30'; 25° 45' S. Brits elevation ranges from 920m-1782m above sea level. The study area was chosen because of known occurrences of expansive soils in the area. This information was obtained from the geochemical mapping program undertaken by the Council for Geoscience between 1992 and 1994. The occurrence of clay minerals in the study area may be attributed to the regional geological setting, climate, hydrology, and geomorphology.

The regional geological setting of the area is comprised of alternating sequences of sandstone and shale of the Pretoria Group, overlain by the Magaliesberg Formation, which consists of coarse quartzite and minor sandstone (Erikson et al., 2006). The Magaliesberg Formation underlies the Bushveld Complex, which is comprised of layered mafic intrusions of the Rustenburg Layered Suite followed by a felsic phase of the Lebowa Granite Suite. The Rashoop Granophyre Suite developed at the contact between the Lebowa granite and the Rustenburg Layered Suite. The granites and the granophyres were emplaced almost simultaneously, and then were intruded by a mafic

portion of the Bushveld Igneous Complex **(**Cawthorn et al., 2006). Outcrops of the Karoo rocks cover a portion of the Bushveld Complex rocks north of Brits. Topographically, the area is relatively flat, with the Magaliesberg quartzite forming a ridge on the southern boundary of the study area. Granophyres occur as hilly topography. The Main Zone gabbros of the Bushveld Complex form prominent hills and thin soils develop on these rocks **(**Cawthorn et al., 2006).

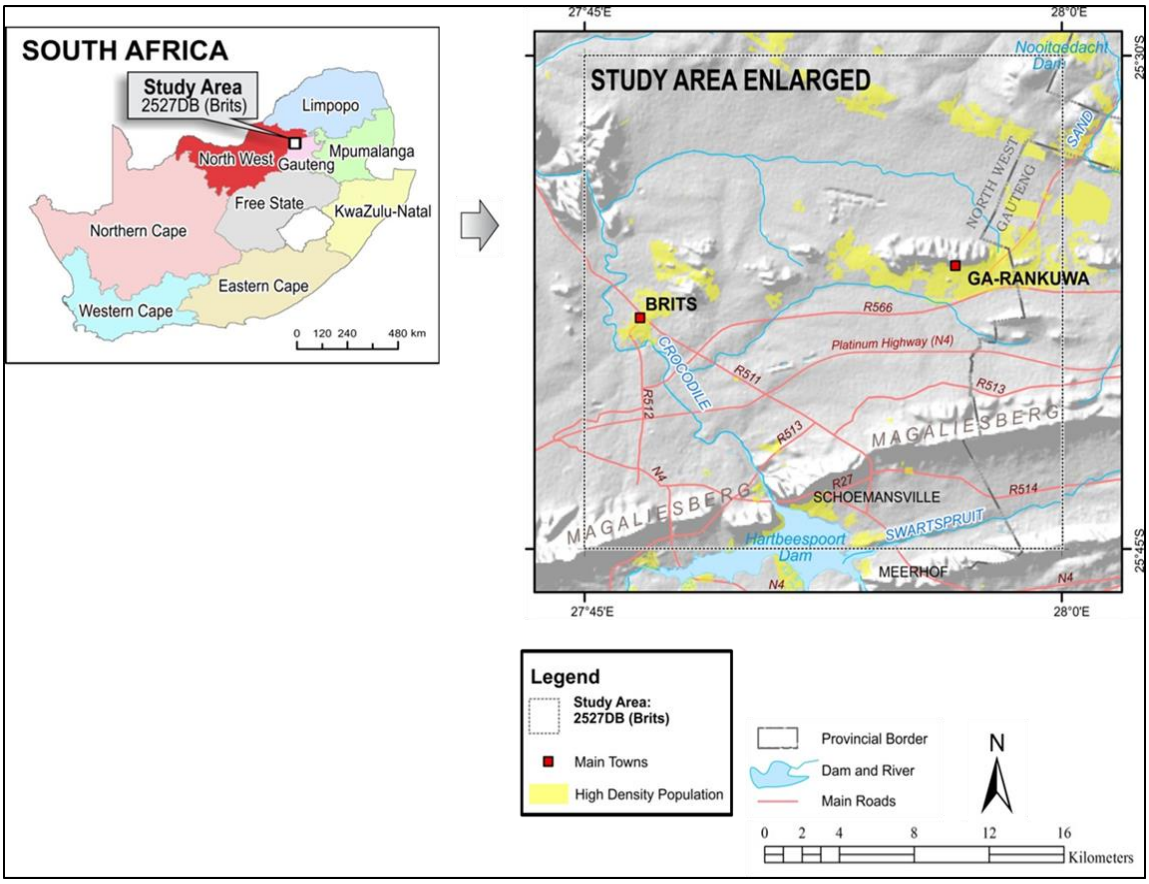

Figure 5: The location of the study area within the North-West Province of South Africa.

According to van der Merwe (1941) cited in de Villiers and Mangold (2002), the main soil types in the North West Province are vertisols, lithosols and lithosolic soils, fersialitic soils. In this study, vertisols are of particular importance. Syers et al (2001) describe them as black cracking clay soils. In this area, they occur in association with melanic and red structured soils. The vertisols in the area can therefore range from red or grey to the more common deep black known as "black cotton". Figure 6 shows two images of soils mostly encountered in the study area. These images were taken under dry weather conditions (18 and 23 November 2012) and the soils were relatively dry.

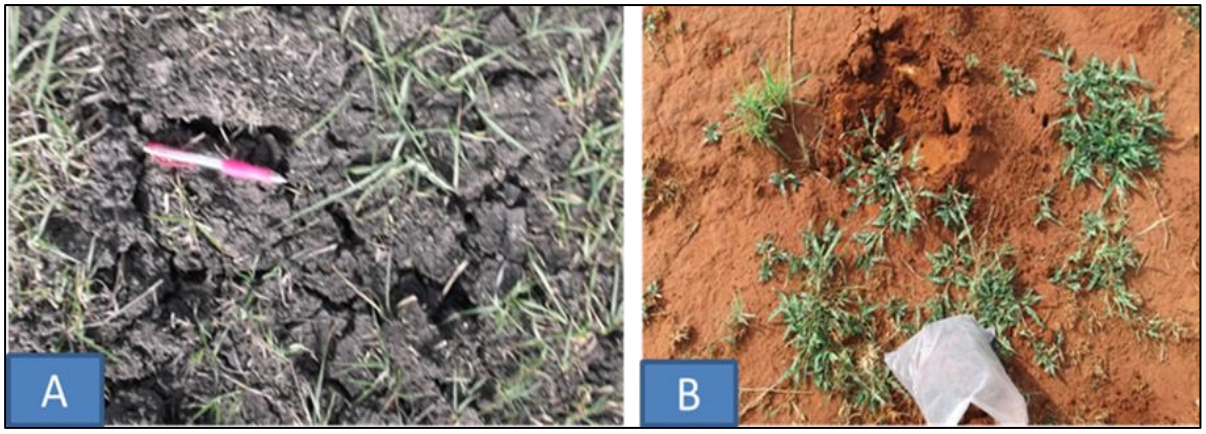

Figure 6: Images of dominant soils in the study area. Image A shows dark coloured soils, strongly structured with desiccation cracks; these soils are associated with expansion. Image B is red structured soil showing no desiccation cracks.

The effect of expansive soils was evident on civil infrastructure such as lightweight buildings, shallow foundations, roads, and pavements in the area. Damages on the structures included cracking, distortion and misalignment of doors and windows. Figure 7 shows pictures taken in the study area illustrating damage to civil infrastructure. The pictures were taken just before the rainy season between 18 and 23 November 2012 except for image C, that was taken from the CGS archives. Figure 8 shows houses built from metal products as a substitute for bricks and cement commonly used, which have proven to be expensive and unstable due to constant cracking and repairs necessary thereafter.

Figure 7: Images from the study area displaying damaged infrastructure associated with expansive soils (image C was taken from CGS archives).

Figure 8: Houses built from metal products as an alternative to the traditional building material (bricks and cement). Note the dark coloured soils associated with expansion.

The North West Province has different climatic conditions from west to east; the study area is in the eastern part of the province that has temperate climate (de Villiers and Mangold, 2002). On average, the eastern part of the province receives about 600mm per annum of rainfall that peaks in early summer (December). Its surface water comprises of rivers, dams, pans, wetlands and dolomite eyes. The North West Province has a large reservoir of underground water in the form of fractured aquifers and dolomitic compartments (de Villiers and Mangold, 2002).

3.2. Method

A summary of the method followed in the study is displayed in Figure 9. Details on the individual steps are described in more detail in Sections 3.2.1 to 3.2.5.

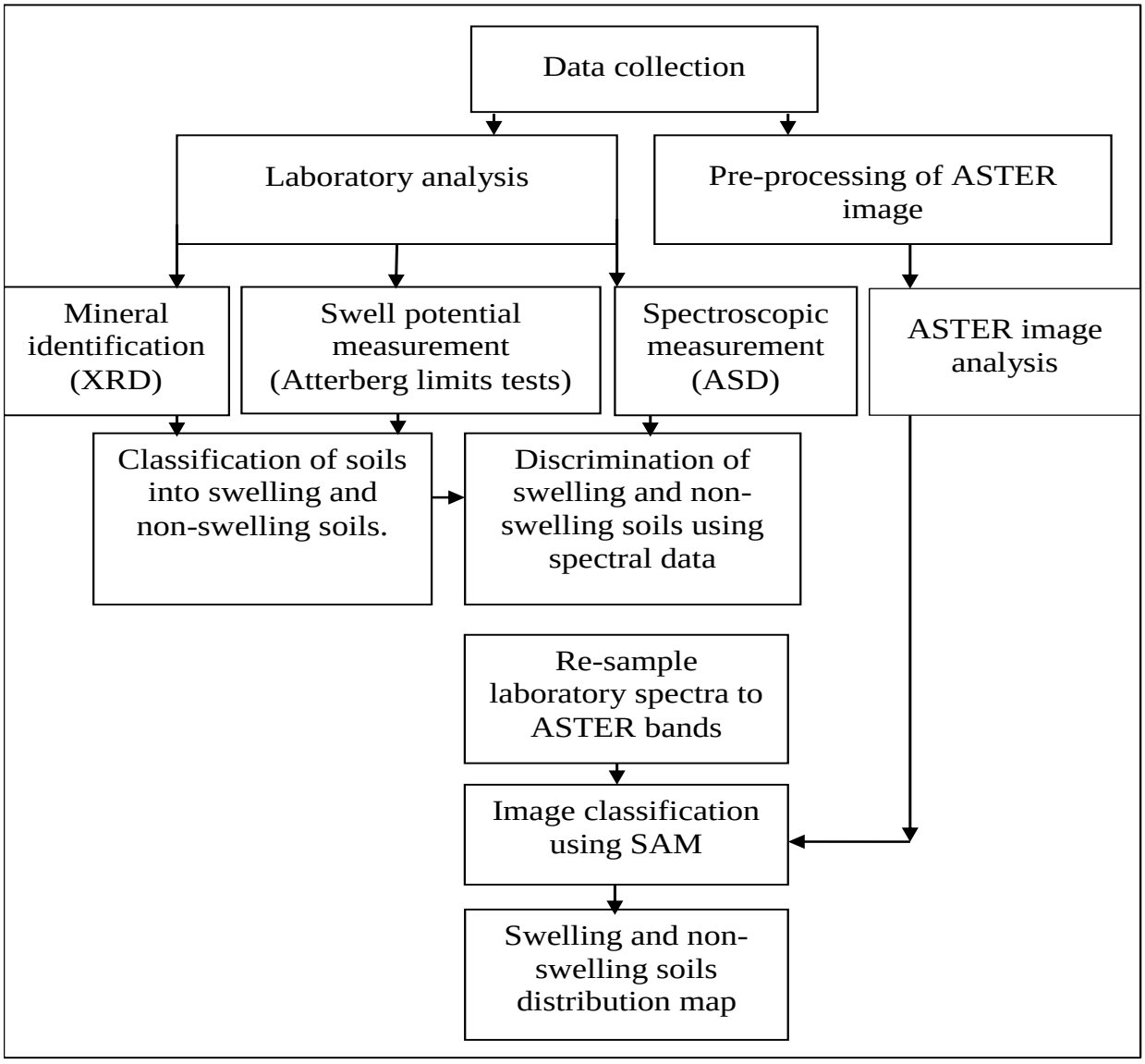

Figure 9: Schematic work flow diagram for this study.

3.2.1. Field data collection

Soil samples were collected in summer between 18 and 23 November 2012 and on the 22nd of January 2013, and coincided with dry weather conditions. A random sampling method was employed and a suite of 53 samples was collected from the top soil to a depth of about 30cm. The distribution of sample points in the study area is depicted in Figure 10. A scoop and a spade were used to collect soil samples of about 5-10kg each. The soil samples collected in the field were generally dry. They were collected into plastic bags, labelled in an ascending order and a Global Positioning System (GPS) was used to record the coordinates of the sampling points. The soil samples were transported to the Council for Geoscience laboratory.

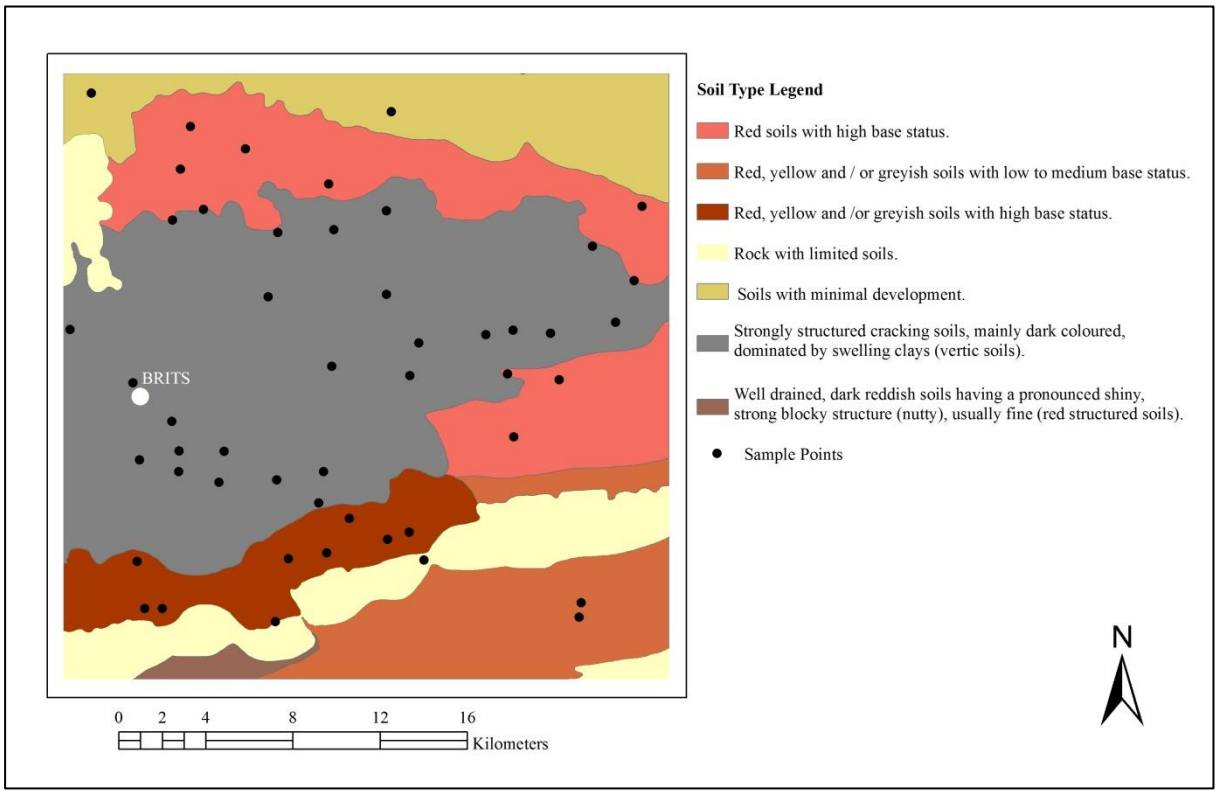

Figure 10: Map depicting sample points within the study area.

3.2.2. Laboratory analysis to determine soil classes (Swelling from non-swelling)

Various laboratory analyses were undertaken to determine different clay compositions of the soil samples. The soil samples were air-dried for several hours to eliminate hygroscopic moisture. Dried soil samples were divided into three portions using a soil splitter. One potion was kept as reference material; another was used for spectroscopic measurements and a third

portion was milled using a swing mill to less than 75 µm particle size and was used for XRD analysis.

Semi-quantitative XRD analysis (Section 3.2.2.1) was completed at the Council for Geoscience (CGS) laboratory, which was used for mineralogical identification. In addition, Atterberg limits tests (Section 3.2.2.2) were carried out at the Soillab laboratory to estimate the swelling potential of soil samples. Spectroscopic measurements (Section 3.2.2.3) were performed at the Council for Scientific and Industrial Research (CSIR) remote sensing black room to detect absorption features associated with specific clay minerals.

3.2.2.1. Mineral identification using X-Ray Diffraction (XRD) analysis

XRD analysis required that the less than 75 µm particle sized samples be further milled to a preferable less than 10 µm fraction. As reported in Loubser and Verryn, (2008) this size is achievable with wet grinding. This is necessary to reduce background noise during analysis. Aliquots of 4g from the less than 75 µm particle size were mixed with 10ml ethanol and ground for 8 minutes in a McCrone micronizing mill. The resulting slurry was oven dried at 40˚C for several approximately eight hours. Figure 11 displays the oven-dried powders, polygonal cracks patterns of the samples are characteristic of expansive soils when dry.

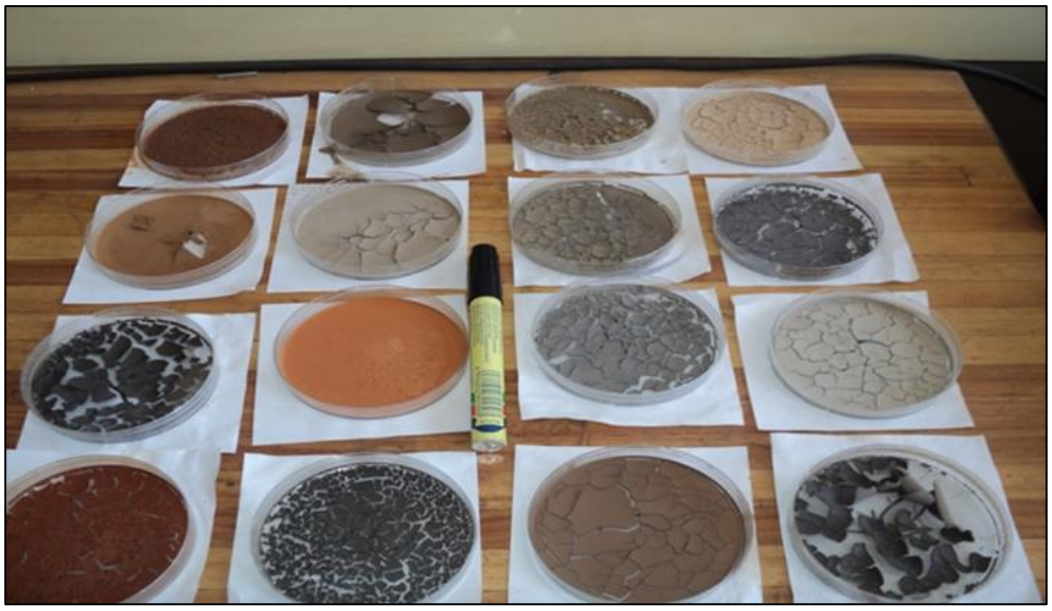

Figure 11: A sample of soil subsamples after being milled in a McCrone micronizing mill and oven dried at 40°C.

The resulting powders were homogenised by light grinding by hand in an agate mortar. The powders were then pressed into plastic holders preparing them to be analysed as whole rock in a BRUKER D8 ADVANCE instrument shown in Figure 12. BRUKER D8 ADVANCE has a 2.2kW Cu long fine focus tube (Cu Kα, λ=1.54060) and 90 position sample changer. The system is equipped with LynxEye detector with 3.7º active area. Samples are scanned from 2 to 70° 2θ at a speed of 0.02° 2θ steps size/3 sec, and generator settings of 40kV and 40mA. Phase identification was based on BRUKER DIFFRAC^{Plus} - EVA evaluation program. The International Centre for Diffraction Data (ICDD) Inorganic/Organic Data base was used for phase search. The ICDD database provides data for material identification and quantification (http://www.icdd.com/).

Figure 12: BRUKER D8 ADVANCE instrument used for XRD analysis.

3.2.2.2. Estimation of swell potential of soil using Atterberg limits tests

Atterberg limits tests were conducted to estimate swell potential of the soil and eventually classify the soil samples as swelling or non-swelling. The Atterberg limits tests conducted were liquid limit, plastic limit and linear shrinkage. Liquid limit and plastic limit tests were

carried out to determine Plasticity index (PI) of soil, which was used to estimate the swelling potential. PI was calculated as a numerical difference between liquid limit and plastic limit of each soil sample. Atterberg limits test followed the standard test procedures of AASTHO specifications (AASHTO, 2000), AASTHO T89 for liquid limits determination, AASTHO T90 for plastic limit and plasticity index, California Test Method 228-A was used to determine linear shrinkage of soil**.**

3.2.2.3. Soil spectroscopic measurements

An Analytical Spectral Device (ASD, 2002) FieldSpec3® was used to take soil spectroscopic measurements. The instrument takes a single spectrum in milliseconds via its fibre-optic input. The light source was a halogen lamp positioned at about 200 mm and inclined at 45° from each soil sample. The ASD collects data in the 350-2500nm wavelength region of the electromagnetic spectrum, which covers the near infrared region and the short wave infrared region with a resampled resolution of 1nm. In the 350-1000nm wavelength region, it has a spectral resolution of 3nm and 10nm for the 1000-2500nm region (ASD, 2002). The spectrometer has one detector in the VNIR and two detectors in the SWIR; this makes ASD suitable for clay analysis since major absorption features associated with clay minerals are found in the SWIR region.

Spectral measurements of air-dried soil samples were taken in a dark room to ensure stable atmospheric and illumination conditions, no sample preparation was needed. However, visible organic materials such as twigs were removed from the subsoil samples. Soil samples were placed on a black paper to control scattering, which might affect the soil spectrum. A white reference panel was used to optimize the ASD, thereby converting DN values to reflectance. Five spectral measurements were collected per sample at different positions. The results were averaged to find the final spectral reflectance value.

3.2.3. Data analysis

3.2.3.1. Discrimination of swelling and non-swelling soils using XRD and Atterberg limits data

The criteria for determining whether a soil sample is swelling or non-swelling considered both XRD and Atterberg limits data. XRD data used the presence of smectite or/and interstratification (mixed-layer clays) to classify soil samples as swelling or non-swelling. Smectite is the only mineral that gives swelling properties to soil (Vede, 1992; Deer 1992; Nesse, 2000). The presence of interstratification content was classified as soils with swelling potential since interstratification is generally associated with the presence of smectite. (Deer, 1992; Vede, 1992; Nesse, 2000). On the other hand, Atterberg limits data classified soil samples based on their plasticity index, which was calculated as a numerical difference between liquid limit and plastic limit. The classification followed Burmister, (1949) soil classification criteria, where soil plasticity classes vary from non-plastic to very high plasticity (Table 3).

Table 3: Soil classification based on plasticity index data (Burmister, 1949)

Plasticity index range	**Plasticity category**	**Potential expansion**
0	Non-plastic	Non-expansive
1-5	Slightly plastic	Low
5-10	Low plasticity	Low
10-20	Medium plasticity	Moderate
20-40	High plasticity	High
>40	Very high plasticity	Very high

3.2.3.2 Statistical techniques used to validate soil classification based on XRD and Atterberg limits data

Indirect and direct statistical techniques were used to validate the classification of swelling from non-swelling clays based on the XRD and Atterberg limits data. The indirect techniques included hierarchical clustering and factor analysis while discriminant analysis was used as a direct technique (Rencher, 2002). Misclassified samples and outlier samples in terms of mineralogy as determined by XRD were excluded from statistical analysis.

Indirect statistical analysis

Hierarchical clustering was used to determine possible soil classes present. The algorithm clusters objects based on their similarity. Each sample is initially designated as a class by itself then samples are joined consecutively together into larger clusters (Rencher, 2002). The maximum distance that connects constituents of a cluster may describe a cluster and hierarchies of clusters are formed at different distances. A dendogram was used to represent the clusters. The Y-axis of a dendogram represents distances at which clusters are formed and X-axis shows the samples.

Factor analysis was used to investigate the relationship between soil samples (variables) being classified and important minerals (factors) classifying them. It is based on principal component analysis and factor analysis (Rencher, 2002). It investigates if a number of variables of interest are linearly related to a few random latent variables. It aims at reducing the redundancy among the variables by using a smaller number of factors when classifying variables into groups. The classification seeks to account for the correlations among the variables (Rencher, 2002).

Direct statistical analysis

Discriminant analysis was used to investigate the success of the XRD/Atterberg classification technique. It determined the most basic way to distinguish between swelling/non-swelling groups. Discriminant analysis allows for the investigation of differences between groups based on the attributes of the cases, indicating which attributes contribute most to group separation (Borradaile, 2003). The following conditions should be satisfied for discriminant analysis to be employed successfully. There must be at least two correctly classified categories; each category must be well defined, clearly differentiated from any other categories. The attribute(s) used to classify the groups should discriminate quite clearly between the groups to minimize or eliminate overlaps. Group sizes of dependent variables should not be completely different and should be at least five times the number of independent variables (Rencher, 2002).

A bootstrapping approach (an iterative re-sampling approach) was adopted to assess the classification accuracy. It was chosen because of the small nature of the swelling (n = 35) and non-swelling (n = 13) classes as determined by the XRD/Atterberg limits test. Bootstrapping is a statistical technique that belongs to a group of resampling methods (Good, 2005). It draws randomly from sample estimates with replacement from the original sample. In this study, 30 bootstrap resamples were drawn, in each iteration 35 swelling soil samples and 13 non-swelling soil samples were drawn. One third of the swelling and non-swelling soil samples were used as validation data and the other two thirds as training data. The classification accuracy was assessed in terms of producers, users, and overall accuracies.

The producer's accuracy is the probability of ground truth points of a land cover being classified by the producer of the map as the same land cover on a map (Congalton, 1991). The user's accuracy is a measure of the likelihood of any classified point selected by a user being representative of the actual land cover class on the ground (Congalton, 1991). The producer accuracy for swelling and non-swelling soils were calculated in a similar way, the same is true for the user's accuracy. The swelling soil class is used for explaining this. Producer's accuracy for swelling soils class was calculated as the total number of correctly classified swelling soil samples divided by the total number of samples classified (Congalton, 1991). The user accuracy for swelling soils was calculated as the total number of correctly classified swelling soil samples divided by the total number of samples classified as swelling (Story and Congalton, 1986).The overall accuracy was calculated by dividing the total number of correctly classified samples (swelling and non-swelling) with the total number of samples.

3.2.4. Discrimination of swelling and non-swelling soils using spectral data

The laboratory measured soil spectra were converted into ASCII files, thereby creating a spectral library of the soil samples. In this study, the 2165nm to 2405nm spectral region was used to classify soil samples. This region was chosen because clay mineral's characteristic absorption features are found in the region1900nm-2500nm (Goetz et al., 2001; Chabrillant and Goetz, 2006). Different authors have chosen different regions within the SWIR region to characterize and classify swelling soils. Chalibrant et al., (2002) discriminated between swelling potential of different soils using 1800-2400nm spectral region. de Senna et al., (2008) classified clay minerals used in the manufacturing industry using 1400nm-2500nm. Yitagesu et al, (2009) used 2100-2420nm region in quantifying engineering properties of

swelling soils. Once the classification of the soil was done, a bootstrapping method (30 iterations) was used to assess the classification accuracy.

3.2.5. Classification of swelling and non-swelling soils from ASTER image

Image analysis for the study area was performed on an ASTER level 3A (Figure 13) scene that covers most part of the study area, the image was acquired on the 30th of July 2004. Figure 13 displays the false colour composite (Red Green Blue, 321) of the image used. Another image that covers the remaining part of the study area was acquired on the 24th of October 2006. The image is highly vegetated and therefore, not suitable for mapping soils.

3.2.5.1. Image pre-processing

The image was radiometrically corrected, crosstalk corrected, rotated, and geometrically co-registered by the image provider. Crosstalk correction is unique to ASTER imagery. Crosstalk is an effect in ASTER imagery caused by signal leakage from band 4 into adjacent bands 5 and 9. It is assumed that this is caused by incident photons of band 4 detector planes being reflected and collected by detectors of the other bands (Van der Meer et al., 2012).

The above-mentioned pre-processing steps performed by the image provider were followed by image format conversion from band-sequential single-band format to stacked, multiband, integer-scaled, band-interleaved format. This conversion is necessary for ACORN atmospheric correction software (Kruse & Perry, 2007). ASTER VNIR bands and SWIR bands do not have the same spatial resolution; VNIR bands have a 15m resolution while SWIR bands have a 30m resolution. To achieve a consistent spatial resolution in the image VNIR 15m were re-sampled to SWIR 30m spatial resolution; the thermal infrared (TIR) bands were not used for analysis in this study.

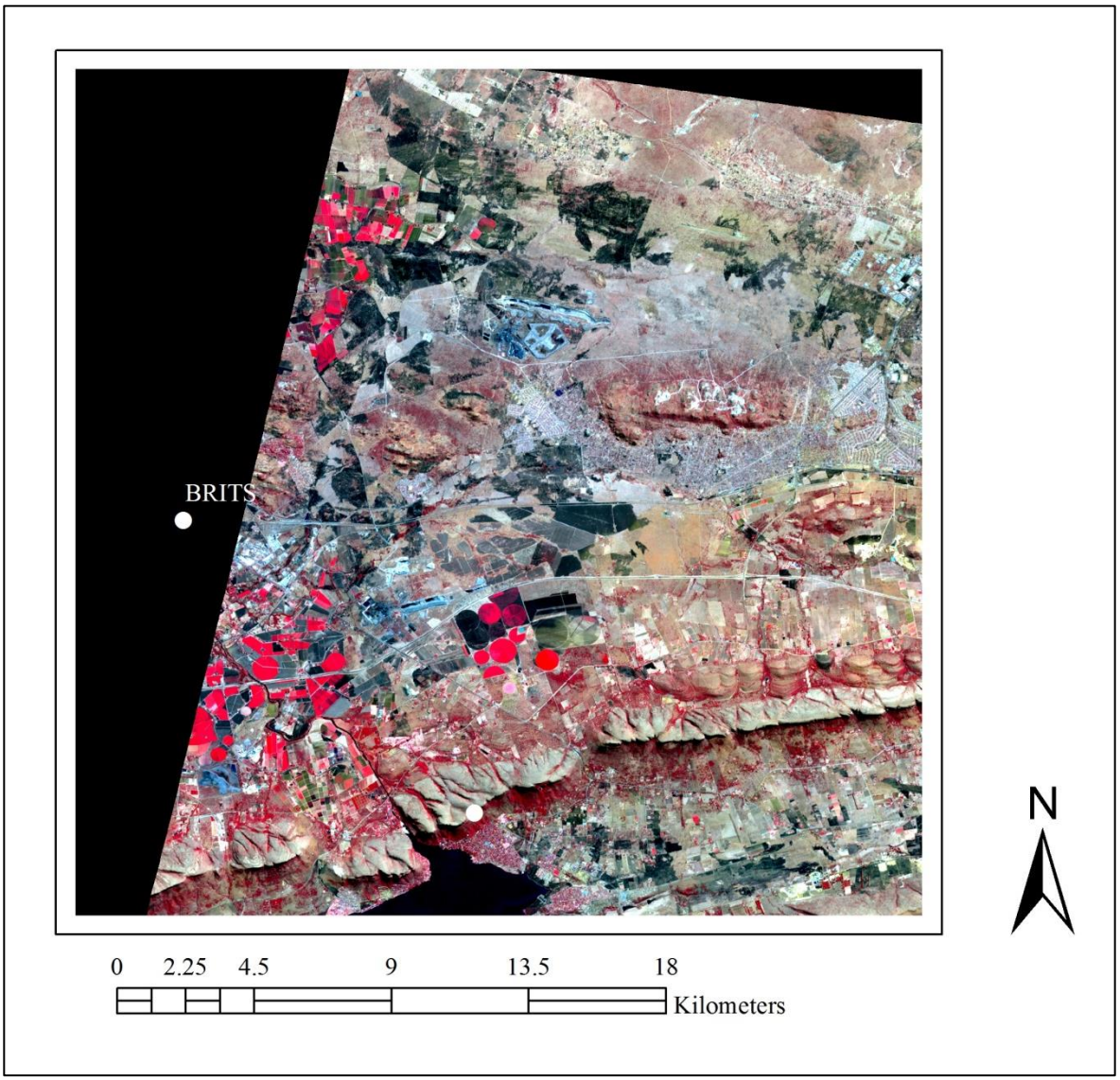

Figure 13: ASTER false colour composite covering parts of the study area.

The next pre-processing step was atmospheric correction, which is a critical technique for removing the influence of atmospheric effects on radiance data. ACORN software was used for atmospheric correction of the image. The software uses licensed MODTRAN-4 radiative transfer code to retrieve surface reflectance without ground measurements. ACORN also contains several artifact suppression options such as automated wavelength adjustment and elimination of noisy channels (AIG, 2001).

3.2.5.2. Image classification into swelling and non-swelling clays

The first step of image classification was the calculation of Normalized Difference Vegetation Index (NDVI) using Equation 4. The NDVI was calculated to create a mask that

excluded pixels dominated by vegetation. NDVI is a widely used index for detection of live green plant cover in multispectral remote sensing data. NDVI values are represented as a ratio ranging from -1 to 1(Jensen, 2005).

$$NDVI = \frac{NIR-RED}{\text{NIR+RED}} \qquad (3)$$

Where, *NIR* is the reflectance in the near infrared band

RED is the reflectance in the red band

A typical range from a not so green area to a very green area would be between -0.1 to 0.6(Jensen, 2005). Values approaching 1 are associated with greater density and greenness of plant cover. Bare soil, rock and snow values are close to zero with a range between -0.1 to 0.1. Negative values of NDVI closer to -1 are indicative of deep water (Jensen, 2005).

Moreover, to the exclusion of pixels dominated by vegetation other land cover types such as water bodies, built-up areas were excluded in order to create a bare soil map. This was done by choosing these land cover types as Regions Of Interest (ROI) and masking them out, thereby creating a bare soil map. The map was used to map out swelling and non-swelling soils in the study area, using laboratory measured spectra.

In order to map swelling and non-swelling soils using an ASTER image using laboratory-measured spectra, spectral re-sampling of laboratory measured spectral data to ASTER bands was performed. Laboratory measured spectral data is hyperspectral with narrow contiguous wavelengths, while ASTER data is multispectral with fewer, broad and wider wavebands (Lillesand et al., 2008). Spectral re-sampling reduced spectral resolution of laboratory spectra into multispectral ASTER bands. Spectral detail was lost during the process of re-sampling and therefore the re-sampled spectra will have a different shape to that of the original measured spectra (Kruse et al., 1993). Average re-sampled spectra for swelling and non-swelling soils were used as endmembers for supervised classification of the image. Spectral Angle Mapper (SAM) supervised classification technique was used in this study. The SWIR bands were used for the classification.

Quantitative accuracy assessment of the image classification could not be performed due to the limited number of non-swelling soils (n = 13) as opposed to swelling soils (n = 35). The non-swelling soil samples were not sufficient to be split into training and validation points. Qualitative accuracy assessment was performed by plotting (ArcGIS10) classified samples and soil contacts as per soil map (Figure 10) of the study area onto the classified image. The image used did not cover the whole of the study area, hence only the samples that plotted on the image were considered for this qualitative accuracy assessment. ENVI provided statistics of the area covered by swelling and non-swelling soils.

Chapter 4. Results and discussions

This chapter presents results on semi-quantitative mineral phase identification using X-Ray Diffraction (XRD) analysis and the estimation of swell potential of the soil using Atterberg limits tests. It further presents results of the spectral classification of swelling and non-swelling soils using ASD spectral reflectance. Lastly, results of classification of distribution of swelling and non-swelling soils using ASTER image.

4.1. Classification of soils using XRD

The first laboratory analysis done to determine soil classes was mineral identification using XRD analysis. Semi-quantitative mineral abundances were calculated by Reference Intensity Ratio (RIR) method (Chung, 1974). A sample of XRD deffractograms showing peaks and their intensities used in calculating mineral abundances is displayed in Appendix B. XRD analysis results are tabulated in Appendix C. The results are expressed as semi-quantitative estimates of the mineral abundances in weight percentages of whole rock analysis. Minerals identified in the study area were clay mineral groups such as chlorite, kaolinite, interstratification and smectite. Clay minerals were identified together with their parent material such as amphiboles, micas, feldspars, and quartz. Other minerals recognized include hematite, goethite, ilmenite, and magnetite. The most dominant mineral identified was quartz; smectite minerals were the most dominant amongst clay minerals.

Smectite or/and interstratifications (mixed-layer clays) classified soils as swelling otherwise non-swelling. Soil samples with smectite minerals and/or interstratification (swelling soil) were found in 69.81% of the samples used for this study. In order to link the distribution of swelling and non-swelling soils to the soil types of the study area, a swelling/ non-swelling distribution map (Figure 14) was created. The map was created by plotting XRD classification results (Appendix D) onto a soil map of the study area. Swelling soils generally had soil colours and texture that varied from red clayey silt, brown, and grey to deep black silty clay. While, non-swelling soils varied from light reddish orange, light red to light brown sandy silt. Please refer to Appendix I for a fieldwork report that describe each sample's recorded colour and texture. In the swelling/non-swelling map (Figure 14) below, black triangles represent soil samples classified as swelling soil, while blue dots represent soils

classified as non-swelling. It is clear that majority of the samples classified as swelling (black triangles) plots on the vertic soils of the map, which was expected. However, not all the samples (both swelling and non-swelling) plotted on the expected soil types on the map. Hence, the classification needed support (Atterberg limits tests) and validation (statistical methods).

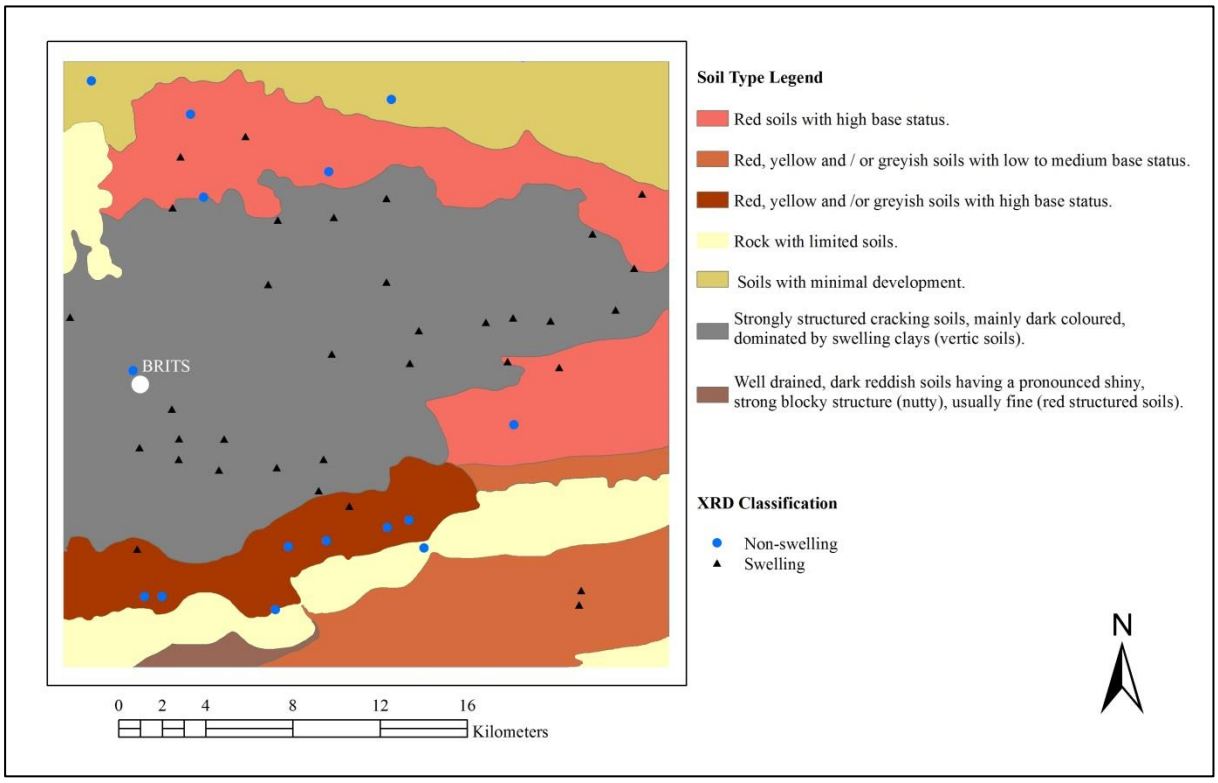

Figure 14: Swelling/ non-swelling distribution map.

4.2. Classification of soils based on Atterberg limits

Atterberg limits tests were conducted to estimate swell potential of soils and to support XRD soil classification. This was important for supporting XRD soil classification such that any soils classified as swelling or non-swelling has the corresponding swelling property (plasticity). Appendix E shows results of the Atterberg limits test conducted, namely liquid limit, plastic limit and linear shrinkage. Liquid limit and plastic limit results were used to calculate plasticity index, which is a numerical difference between them (Equation 2). The plasticity index was used to estimate swell potential of each soil sample following Burmister (1949) classification method. Results show that soil plasticity in the study area ranges from non-plastic soils to soils with very high plasticity. Table 4 show plasticity index range,

plasticity index categories, and number of samples in each category, percentage of each category and potential expansion of each class.

Table 4: Classification of soil according to plasticity index modified after Burmister (1949).

Plasticity index range	Plasticity category	Potential expansion	Frequencies	Percentage (%)
0	Non-plastic	Non-expansive	4	7.55
1-5	Slightly plastic	Low	2	3.77
5-10	Low plasticity	Low	6	11.32
10-20	Medium plasticity	Moderate	17	32.08
20-40	High plasticity	High	23	43.40
>40	Very high plasticity	Very high	1	1.89

To correlate plasticity data to the soil types of the study area and eventually to the swelling/ non-swelling distribution pattern, a plasticity index map was created (Figure 15). This map was created in a similar way to that of the swelling / non-swelling distribution map (Figure 13), by plotting plasticity index values onto a soil map of the study area. Generally, moderate to high plasticity values plotted on the vertic soil, while non-plastic to low plasticity plot outside this region.

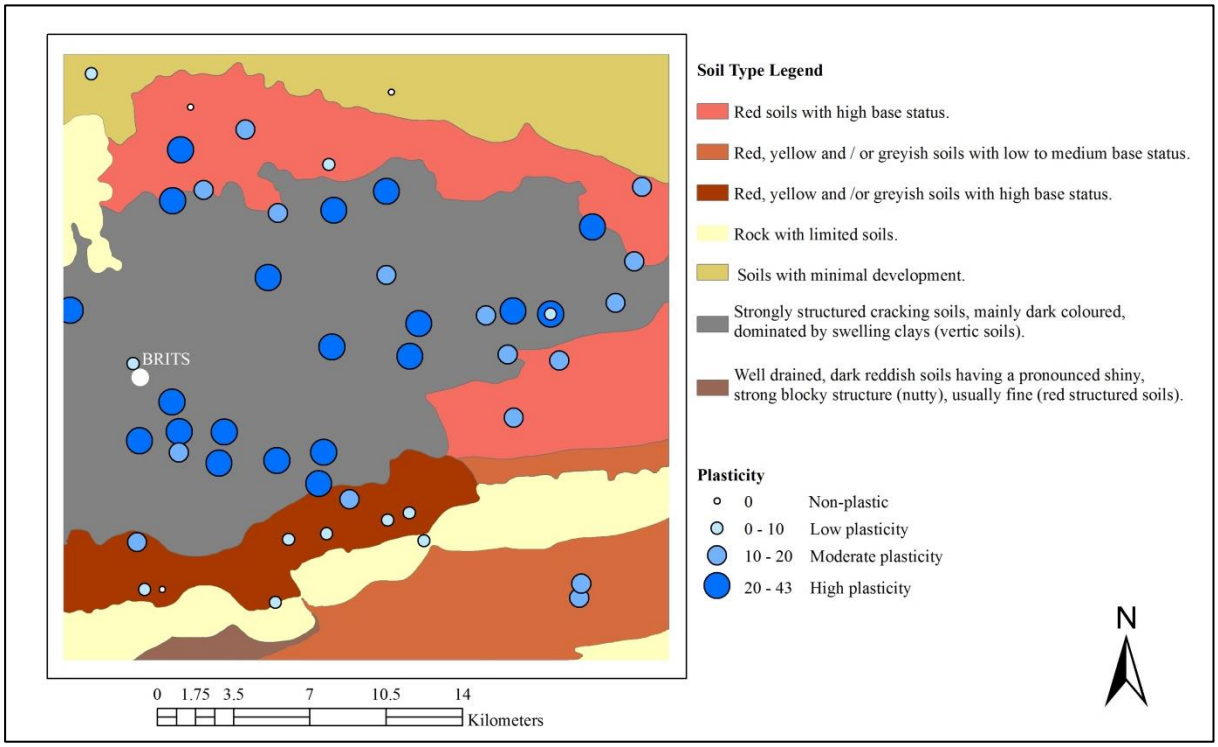

Figure 15: Plasticity index map showing variation in plasticity, from non-plastic to very high plasticity within the study area.

4.3. Soil classification based on XRD and Atterberg limits results

Soil samples were firstly classified based on XRD results (Appendix D), then were classified based on plasticity index (Appendix E). Finally, they were classified based on both XRD results and Atterberg limits data (Table 5). The final classification (Table 5) showed that generally soils with smectite or/and interstratification have medium to very high plasticity and are swelling. On the other hand, soils without smectite or/and interstratification exhibit low plasticity or non-plastic behaviour and are classified as non-swelling. Three samples out of the 53 samples analysed did not conform to the pattern and were considered misclassified.

Table 5: Discrimination of swelling and non-swelling soils using XRD and Atterberg limits data.

Sample	Interstratification	Smectite	Plasticity Index (PI)	Final classification
1	-	-	5	non-swelling
2	-	-	NP	non-swelling
3	5	-	13	swelling
4	-	35	30	swelling
5	7	-	15	swelling
6	-	19	19	swelling
7a	19	-	25	swelling
7b	15	10	SP	miss-classified
8	7	18	23	swelling
13	-	31	20	swelling
14	8	15	33	swelling
15	9	-	22	swelling
18	15	11	20	swelling
19	-	37	21	swelling
20	-	-	17	miss-classified
21	3	-	30	swelling
23	-	-	10	non-swelling
24	11	9	15	swelling
25	-	-	NP	non-swelling
26	4	-	28	swelling
27	-	-	8	non-swelling
28	-	-	13	swelling
29	-	-	8	non-swelling
30	4	2	8	non-swelling
31	-	38	6	non-swelling
32	-	34	14	swelling
33	-	45	37	swelling
34	-	36	25	swelling
35	3	-	33	swelling
36	-	-	34	swelling
37	-	-	15	swelling
38	-	-	10	non-swelling
39	-	56	10	non-swelling
40	-	48	8	non-swelling
41	-	37	38	swelling
42	-	58	34	swelling
43	6	-	29	swelling
44	-	51	43	swelling
45	4	7	14	miss-classified
46	-	22	14	swelling
47	3	-	36	swelling
48	-	30	13	swelling
49	-	14	24	swelling
50	-	56	14	swelling
51	14	8	36	swelling
52	-	44	19	swelling
53	7	-	31	swelling
54	-	-	20	swelling
55	-	-	34	swelling
66	-	-	17	swelling
75	-	-	SP	non-swelling
76	-	-	NP	non-swelling
77	-	-	NP	non-swelling

4.4. Statistical techniques used to validate the classification of soils based on XRD and Atterberg limits data

4.4.1. Hierarchical clustering of soil samples

Hierarchical clustering of XRD results data produced three clusters displayed on a dendrogram (Figure 16). Appendix F tabulates the cluster's properties such as within-class variance and minimum distance to centroid. On the dendrogram (Figure 16) sample names/numbers in each cluster are displayed on the horizontal axes. These clusters represent swelling and non-swelling soil classes. Cluster 1 (green) is non-swelling soils, Cluster 2 (pink) is swelling soils and Cluster 3 (maroon) is swelling soils with high iron content. Vertical axis represents similarity among the clusters. The higher the height linking classes the more dissimilar the classes are.

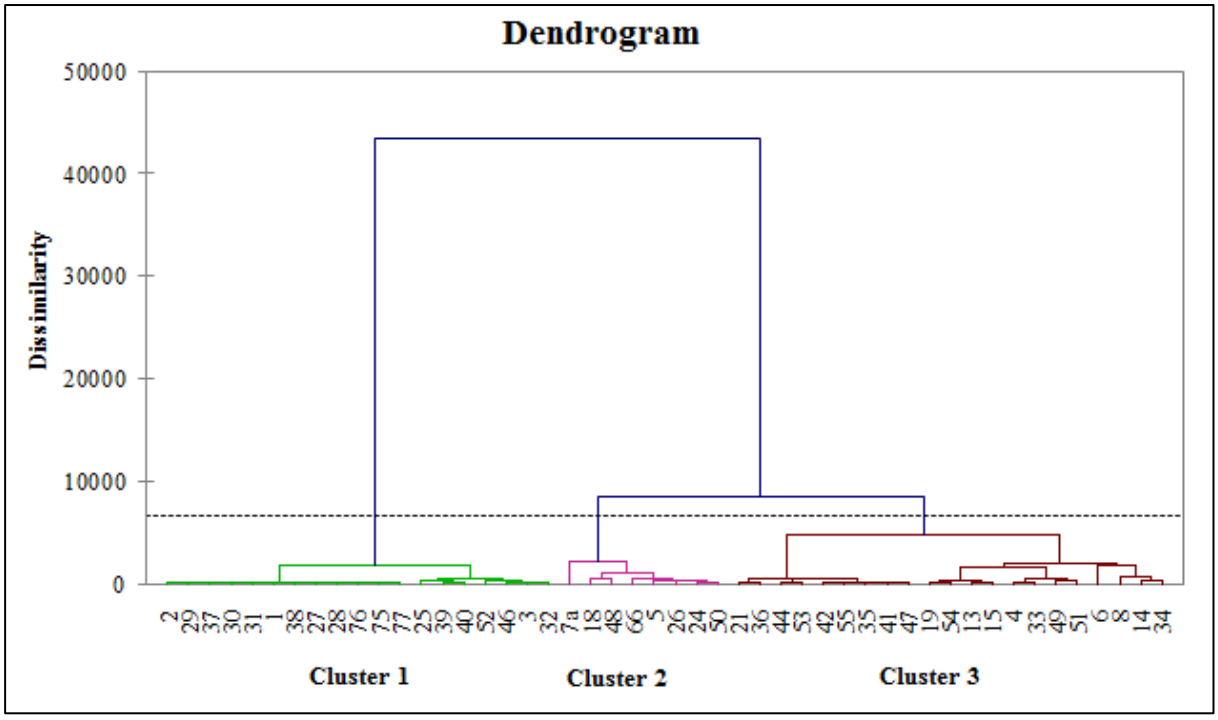

Figure 16: Dendogram displaying results of hierarchical cluster analysis of XRD data.

4.4.2. Factor analysis of soil samples

Factor analysis was used to determine factors (minerals/mineral groups) important in the classification of soil samples (variables) into swelling and non-swelling soils. Factor analysis uses a smaller number of factors that explains the most variation within the variables when

classifying variables into groups. A measure of variation accounted for by a factor is reported as eigenvalues. The higher the eigenvalue of a factor the more variation is explained by that factor. Only factors with percentage eigenvalues greater than 1 were retained (Kaiser, 1960) and used for interpretation of the variation. Table 6 shows the 5 factors retained and their percentage variability and cumulative variability. Appendix G shows correlations between minerals and these factors.

Table 6: Eigenvalues of five factors showing variability of each factor and cumulative variability, the factors accounts for 59.97% cumulative variability.

	F1	**F2**	**F3**	**F4**	**F5**
Eigenvalue	2.94	2.85	1.76	1.36	1.28
Variability (%)	17.31	16.74	10.36	8.00	7.56
Cumulative %	17.31	34.05	44.41	52.41	59.97

Factor 1 represents non-swelling soils, largely characterised by primary silicates such as quarts and mica, positively correlated in factor 1and 2. Factor 2 is the only factor representing swelling soils and associated with smectite and iron rich minerals such as hematite/goethite. Factor 3 is linked to non-swelling clays such as kaolinite/chlorite. Factor 4 is associated with carbonate minerals such as calcite. Factor 5 represents non-swelling soils, highly correlated with iron minerals. The 5 factors account for 59.97% cumulative variability. Factor 1 and 2 together accounts for the highest cumulative variability of 34.05%. A bi-plot displaying factor 1 and 2 mineral association is shown in Figure 17.

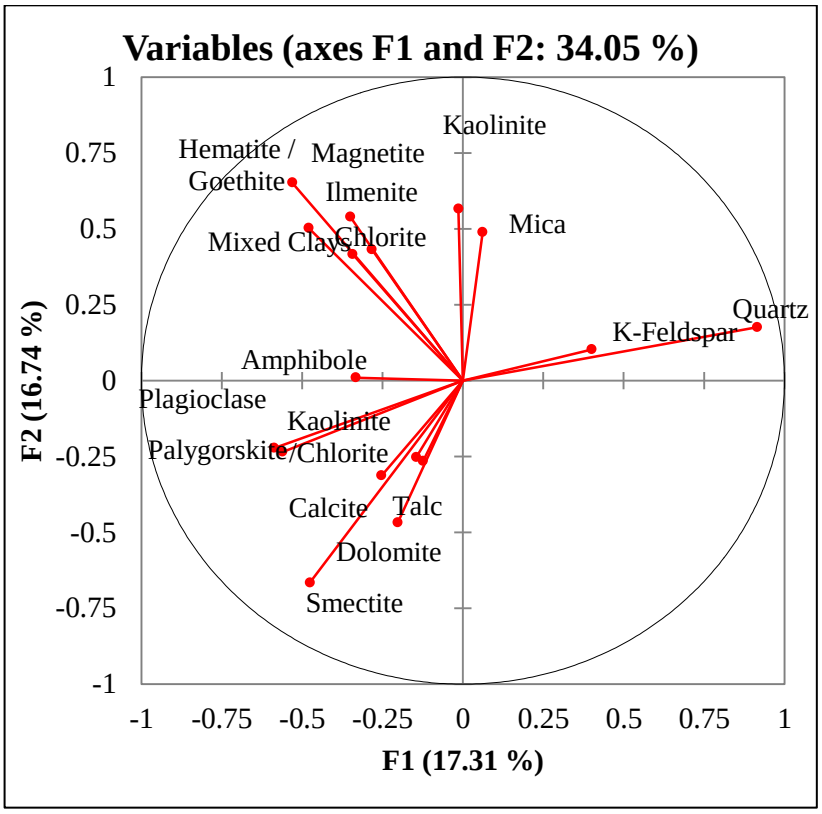

Figure 17: Bi-plot displaying a relationship amongst minerals and factor 1and 2. Factor 1accounts for 17.31% and factor 2 accounts for 16.74 % of the variability.

A relationship amongst swelling and non-swelling soil samples as portrayed by factor 1 and 2 demonstrated on Figure 18. Samples that have similar mineralogy plot closer to each, while dissimilar samples plot further apart.

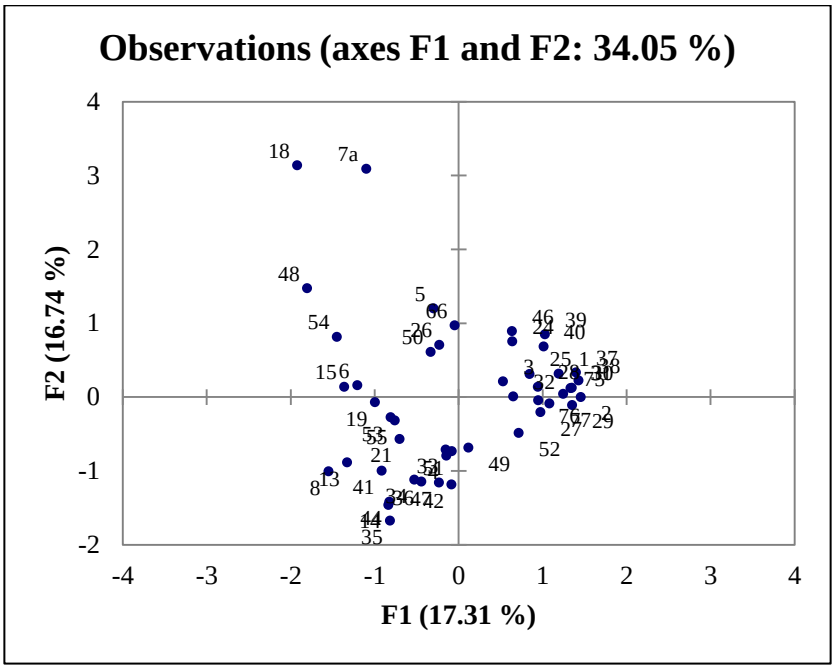

Figure 18: Bi-plot showing relationship amongst swelling and non-swelling soils as depicted by factor 1 and 2. The closer the samples are the more similar their mineralogy is, the opposite is true for distant samples.

4.4.3. Validation of XRD/Atterberg limits classification through discriminant analysis

Discriminant analysis was used to validate the success of XRD/Atterberg limits classification. This was done by creating a discriminant function from the XRD/Atterberg limits classification results. The discriminant function (Table 7) was used to predict membership for the soil samples as either swelling or non-swelling. The classification resulted in two classes; swelling (72.92%) and non-swelling soil (27.08%).

Table 7: Summary statistics of a discriminant function used to predict if a soil sample is swelling or non-swelling.

Categories	Frequencies	%
1(non-swelling)	13	27.08
2(swelling)	35	72.92%

Predicted swelling and non-swelling classification results were cross-validated to test the accuracy of the predictive model. In the cross-validation, each training data is treated as the

test data, and then re-classified to verify the classification. Cross validation results (Table 8), are presented in a form of a confusion matrix. Each column of the matrix represents predicted class, while each row represents the actual class. Results show that only 53.85% of non-swelling soils were correctly classified, meaning only 7 samples from the 13 predicted are actually non-swelling. While swelling soils were, 100% correctly classified. The overall classification accuracy was 87.50%, calculated as correctly classified samples (42) divided by the total number of samples classified (48).

Table 8: Cross validation confusion matrix of discriminant analysis of spectral data.

from \ to	**Non-swelling**	**Swelling**	**Total**	**% correct**
Non-swelling	7	6	13	53.85%
Swelling	0	35	35	100.00%
Total	7	41	48	87.50%

4.5. Laboratory reflectance spectroscopy results

Spectroscopic measurements were acquired to detect swelling soils through identifying absorption features associated with swelling clay minerals (smectite and /or interstratification). Laboratory reflectance spectra of the soils (Appendix I) were subjected to qualitative analysis, with a particular interest in the SWIR where absorption features associated with clay minerals occur. Qualitative analysis involved comparing laboratory measured absorption feature properties with literature values (Clark et al., 1990). Laboratory measured soil spectra showed similar and different spectral characteristics. Similar spectral characteristics noted were the moderately rising convex slopes with increasing reflectance intensity from the VNIR to SWIR wavelength region. Differences noted were in the number of absorption features, their positions, shapes, depth, symmetry, and reflectance intensities.

Three laboratory-measured soil spectra (Figure 19) were chosen to demonstrate major absorption features associated with clay minerals, such as kaolinite (non-swelling), smectite and interstratification (swelling). The chosen soil spectra are generally indicative of all the clay minerals in question. The mineralogy of the samples as determined by XRD is shown in Table 9. XRD results are expressed as semi-quantitative estimates of the phase abundances in weight percentages of whole rock analysis. Semi-qualitative assessment of the soil spectra (Figure 19) indicated that the soil's constituents include primary silicates such as quartz, oxides and hydroxides, clay minerals and water. Note different absorption feature positions, shapes, and numbers, depth, symmetry, and reflectance intensities.

Table 9: Mineralogy (as per XRD results) of the three spectra used to demonstrate major absorption features associated with clay minerals in this study.

Sample	Hematite / Goethite Fe2O3 / Fe+3O(OH)	Ilmenite Fe+2TiO3	Calcite CaCO3	Dolomite CaMg(CO3)2	Gypsum CaSO4•2H2O	Amphibole Ca2(Mg,Fe+2)5Si8O22(OH)2	K-Feldspar KAlSi3O8	Plagioclase Na(Si3Al)O8	Quartz SiO2	Mica KAl2(Si3Al)O10(OH,F)2	Talc Mg3Si4O10(OH)2	Chorite (Mg,Al)6(Si,Al)4O10(OH)8	Kaolinite /Chorite	Kaolinite Al2Si2O5(OH)4	Smectite Ca0.2(Al,Mg)2Si4O10(OH)2•4H2O	Interstratification (Mixed-layer clays)
s7a	7	-	-	-	-	-	-	-	15	11	-	10	-	38	-	19
s8	-	-	23	-	-	-	-	14	20	-	5	-	12	-	10	15
s43	-	13	-	-	5	-	4	-	41	-	-	-	-	-	37	-

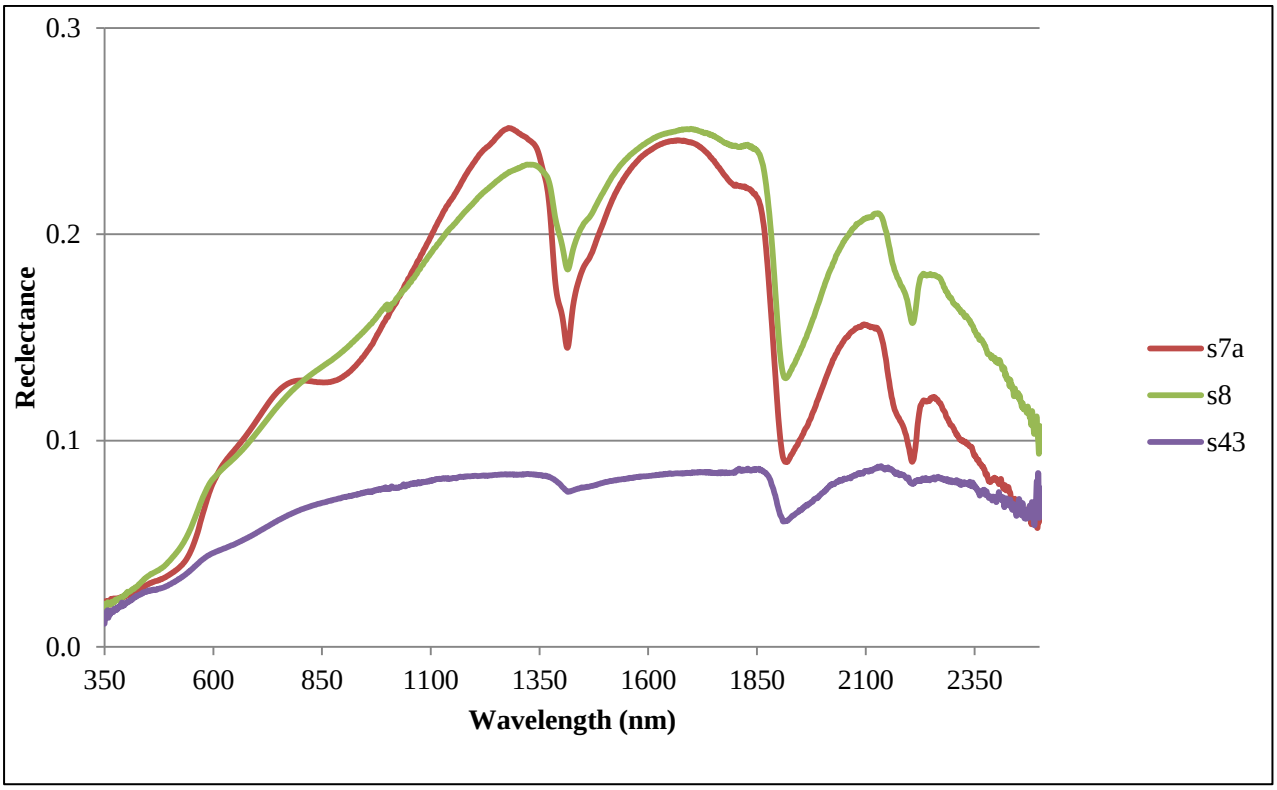

Figure 19: A sample of the laboratory measured soil spectra showing different absorption features associated with clay mineralogy in the study area.

As illustrated in Figure 19 sample s7A displays absorption features associated with kaolinite group minerals and interstratification at 1407nm, 1906nm and at 2201nm. Kaolinite group minerals show the doublets absorption features at1407nm and 2201nm, with a broad absorption and a sharper deeper band at slightly longer wavelength. An additional band due to interstratification was observed at 2349nm. Furthermore the features associated with oxides and hydroxides were observed between 400-980nm, these are due to the hematite/goethite present in the sample.

Sample s8 (Table 9) has kaolinite/chlorite, smectite and interstratification, absorption features associated with these minerals can be seen (Figure 19) near 1409nm, 1900nm and 2200 of the electromagnetic spectrum. The doublets absorption features associated with kaolinite group minerals confirmed the presence of kaolinite in the sample. XRD results (Table 9) reported kaolinite/chlorite since it could have been one or both of these minerals.

Sample s43 (Figure 19) does not show well defined absorption features except for the absorption feature at 1900nm, which is associated with molecular water and is indicative of high swell potential. This is consistent with the mineralogy of the sample (Table 9) which indicated that the sample has high smectite content and therefore is highly expansive. The spectrum of the sample is generally flat and be attributed to the high quartz content in the sample. Furthermore, the sample is of a dark brown colour (Appendix I), which suggests the presence of organic matter.

The mean reflectance spectra for swelling and non-swelling soils were calculated to evaluate differences between them. The averaged spectra do not include misclassified and outlier samples in terms of mineralogy as determined by XRD. The two mean reflectance spectra (Figure 20) show that swelling soils have a lower average reflectance spectrum at all wavelength compared to the non-swelling soils. The lower reflectance spectrum of swelling soils could be attributed to the higher smectite content in swelling soils. Higher smectite content is associated with structural water and higher organic content that can generally give soils a darker colour. In contrast, non-swelling soils are generally brighter in colour (Appendix I) and have high albedo.

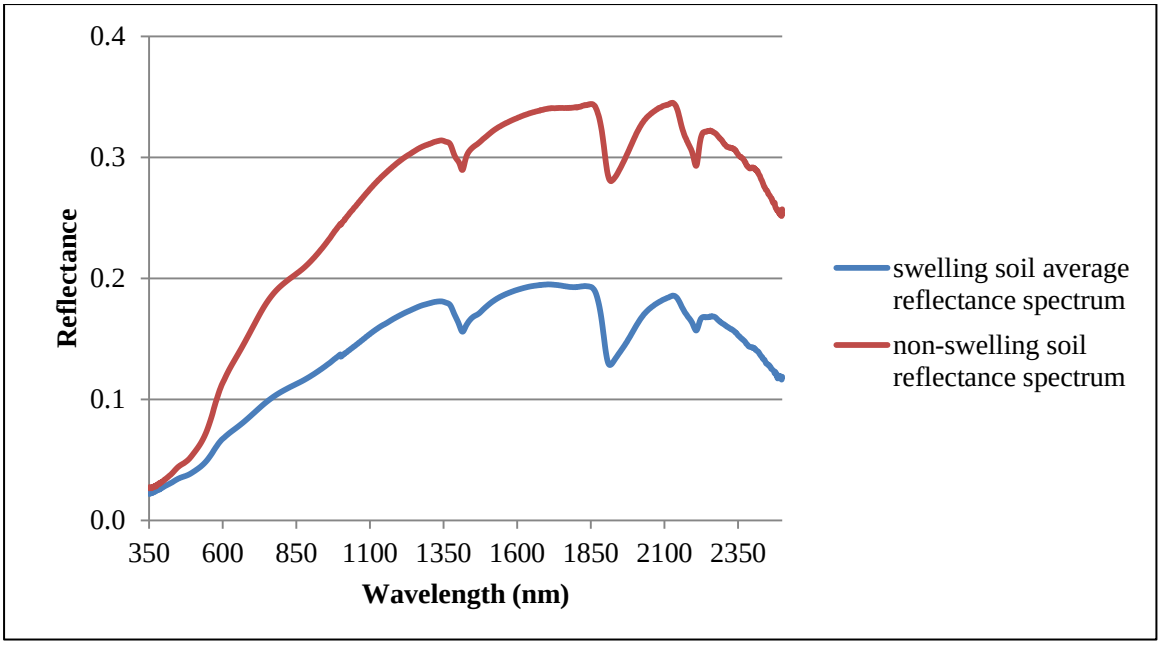

Figure 20: Swelling and non-swelling soils average reflectance spectrum.

4.5.1. Discrimination of swelling soils from non-swelling based on spectral data

The 2165nm to 2405nm spectral region was used for the discrimination of swelling soils from non-swelling soil's spectra. The discriminant function created previously (Table 7) was used to predict membership for this discriminant analysis. The results were cross-validated (Table 10) and show that only 30.77% of non-swelling soils were correctly classified, while only the swelling soils are all (100%) correctly classified. The overall accuracy of the re-classification is 81.25%. The results further show that non-swelling soils were difficult to classify compared to the swelling soils. Non-swelling soils have a low percentage of correctly classified non-swelling soils. This can be attributed to limited number of non-swelling soils available for this study.

Table 10: Cross validation confusion matrix of discriminant analysis of spectral data.

From \ to	Non-swelling	Swelling	Total	% correct
Non-swelling	4	9	13	30.77%
Swelling	0	35	35	100.00%
Total	4	44	48	81.25%

4.5.2. Bootstrapping accuracy assessment

Bootstrapping method (30 iterations) was used to assess the classification accuracy of the soil spectra. In each interaction, 35 swelling soil samples and 13 non-swelling soil samples were drawn. Swelling soils had an average producer accuracy of 71.92% and a standard deviation of 19.57 and an average user's accuracy of 72.92 and a standard deviation of 26.06. Non-swelling soils had an average producer accuracy of 78.23% and a standard deviation of 20.79% and an average user's accuracy of 76.51% and a standard deviation of 19.68%.

4.6. Remote sensing based soil classification using SAM

Classification of the ASTER image (Figure 22) into swelling and non-swelling soils was performed using Spectral Angle Mapper (SAM) supervised classification. Re-sampled average spectral reflectance data for swelling and non-swelling soils were used as endmembers to map the two types of soil. Table 11 shows mean re-sampled spectral reflectance of swelling and non-swelling soils at corresponding ASTER bands. The two mean reflectance spectra show that swelling soils have a lower average reflectance spectrum at all wavelengths compared to the non-swelling soils. Re-sampled spectra (Figure 21) have coarser spectral resolution compared to the original laboratory measured spectra (Figure 20). Re-sampled spectra have fewer, broader, wider spectral bands and the shape differs from that of the original spectra.

Table 11: Re-sampled spectral reflectance of swelling and nom-non swelling soils (averages) at corresponding ASTER bands.

Wavelength (nm)	Swelling soil average spectral reflectance	Non-swelling average spectral reflectance
560	0.06	0.08
660	0.09	0.14
810	0.12	0.19
1660	0.21	0.32
2170	0.19	0.29
2210	0.17	0.27
2260	0.18	0.30
2340	0.17	0.28
2400	0.15	0.27

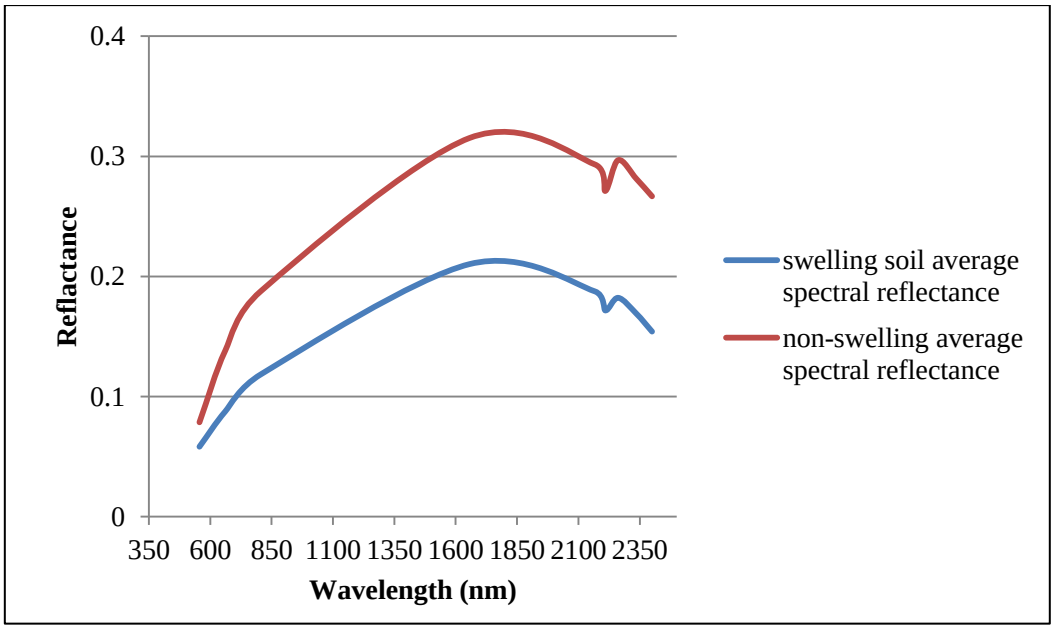

Figure 21: Re-sampled mean reflectance spectra of swelling and non-swelling soils.

Classified samples and soil contacts/boundaries as per soil map of the area were overlaid onto the classified image (Figure 21). This was performed to correlate spatial patterns that exist amongst the classified ASTER image, classified samples and soil map. Soil contacts/boundaries are drawn in a pink colour. Swelling soils are represented by a red colour, non-swelling soils are shown in green colour, and black colour displays unclassified areas. Sample points representing swelling soils are shown in orange/mustard colour dots, yellow points represents non-swelling soils and

misclassified samples are displayed as white dots. Only 45 samples plotted within the available classified ASTER image, 8 samples plotted outside the image and were not considered.

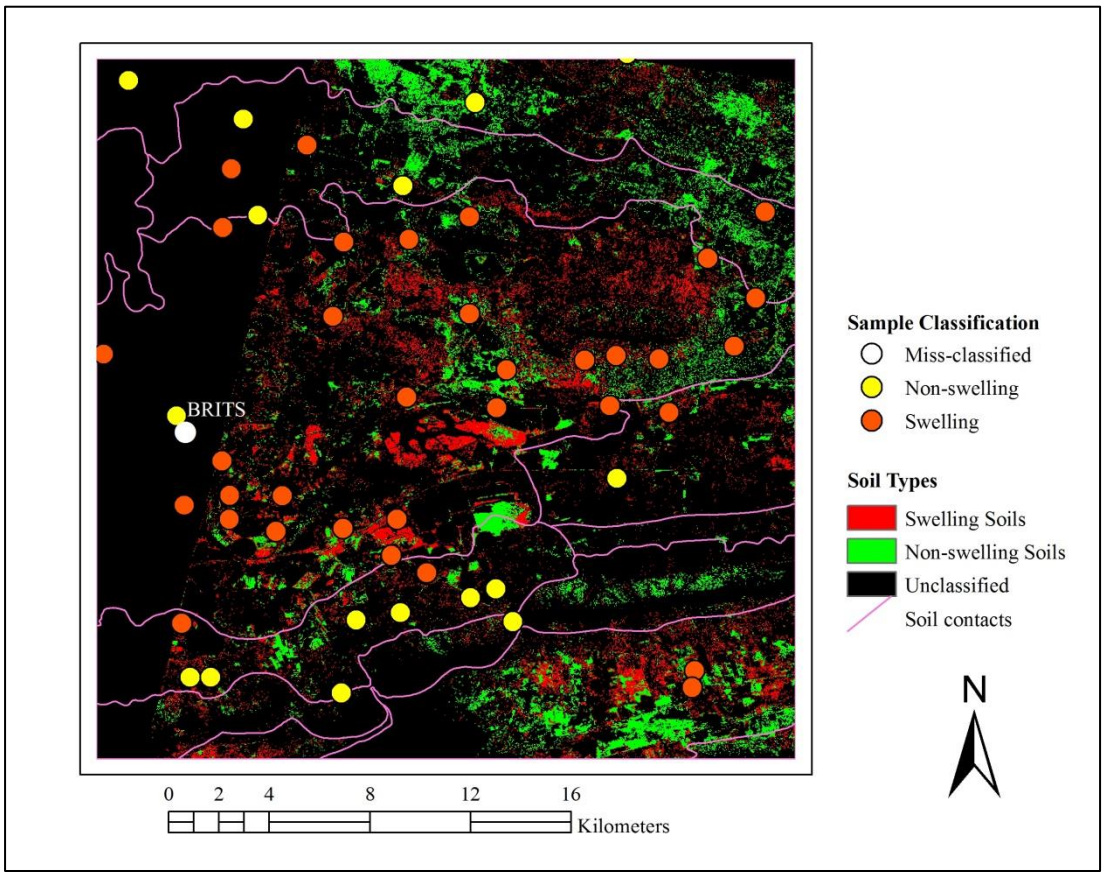

Figure 22: Classified ASTER image showing distribution swelling soils in red, non-swelling soils in green and unclassified areas in black and corresponding classified sample points as per the map legend .Soil contacts (boundaries) overlaid in pink.

Results show that only 2 out of the 11 non-swelling soils plotted on the corresponding non-swelling soils on the classified ASTER image, in terms of percentage this is 18.18%. Swelling soils had a percentage of 68.75% of samples plotting on the corresponding swelling soils. This means 22 out of the 32 swelling soils plotted on the swelling soils region.

The statistics of the area covered by swelling, non-swelling soils and unclassified area were obtained from ENVI and are displayed in table 13. The results area further summarized in Figure 22.

Table 12: Area covered by swelling, non-swelling soils and unclassified area as per SAM supervised classification.

Soil Type	% coverage	Area (km²)
Swelling soils	42.68	239
Non-swelling soils	30.36	170
Unclassified	26.96	151

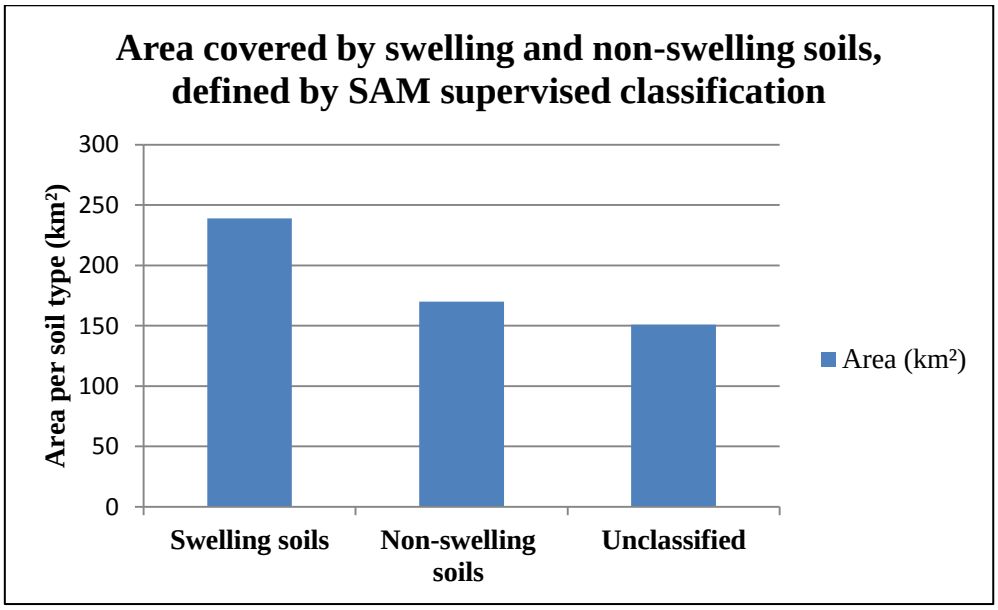

Figure 23: Area covered by swelling, non-swelling soils and unclassified area as defined by SAM supervised classification.

Chapter 5. Findings and recommendations of the study

This chapter presents the main findings, which include scientific contributions of the study. It further presents limitations and recommendations to the study. The findings are presented in relation to the main aim of the study and the specific objectives set to guide the research. Generally, the main aim of the study was to identify and map expansive soils by use of multi-disciplinary techniques. These techniques included traditional methods such as XRD and Atterberg limits tests. Then, the remote sensing techniques were used such as laboratory spectroscopic measurements and multispectral imagery (ASTER). The findings of the study clearly demonstrated that more could be done on the subject and appropriate recommendations for further studies were made.

5.1. Findings of the study

Mineral identification using XRD analysis was carried out in order to identify swelling soils, through identification of swelling clay minerals (smectite and/or interstratifications). The presence of smectite or interstratifications (mixed-layer clays) classified soil samples as swelling or non-swelling. Based on the classification results, swelling soils samples were 69.81%. To support this classification, Atterberg limits tests were conducted to estimate swell potential of soil based on soil plasticity. Soil plasticity in the study area varied from non-plastic to very high plasticity. Soils with medium to very high plasticity were found to be 77.36%. This supports XRD classification results that showed that swelling soils dominates in the study area. The soil samples were further classified based on both XRD and Atterberg limits data. This classification showed that 27.08% of the soils were non-swelling soils, while 72.92% were swelling soils. To validate this classification, statistical technique such as hierarchal cluster analysis, factor analysis and discriminant analysis were employed.

The first statistical technique used was the hierarchical clustering, which resulted in three clusters. Swelling and non-swelling classes were identifiable from hierarchical

clustering results, even though the dendrogram displayed three clusters. The additional class was recognised as swelling soils with high iron content. Factor analysis was used to determine important minerals/ mineral groups in the discrimination of swelling and non-swelling soils. Important minerals for the non-swelling class were the primary silicates such as quarts, mica and k-feldspar. The key factor for the swelling soil class was smectite. Factor analysis results further confirmed that iron rich minerals such as magnetite, hematite/goethite, and ilmenite were an important factor in the mineralogy of the samples. Lastly, discriminant analysis was used to investigate the success of XRD\Atterberg limits classification. According to the discriminant analysis, the overall accuracy of the classification was 87.50%, with 53.85% of non-swelling soils correctly classified and 100.00% accuracy for swelling soils classification.

To correlate soil classification to the soil types of the study area, a swelling/non-swelling and plasticity index map were created. The two maps showed similar patterns. Swelling soils with moderate to high plasticity values plotted on vertic soils. This supported the observation by McKeen, 1992; Chen, 1998; & Olsen et al., 2000 that smectite provides a useful guide for swelling potential. It further corroborates with Deer, (1992); Vede (1992); Nesse, (2000) also stated that interstratification generally swells because of smectite content. In the field, these soils were recognized polygonal desiccation cracks pattern, symptomatic of the presence of swelling clay minerals. The colour of these soils ranged from a reddish brown, brown, grey to black colour.

Once mineral identification and classification using traditional methods (XRD and Atterberg limits) were done, remote sensing techniques were employed. Spectroscopic measurements were taken under laboratory conditions using an ASD collects data in the 350-2500nm region. In the near infrared region absorption features associated with iron oxides and hydroxides such as hematite and goethite respectively were observed. In the SWIR region clay minerals such as kaolinite, smectite and/or interstratifications were identifiable. Interstratification was identifiable as illite/smectite interstratification. Illite/smectite interstratification is the most common one in South Africa (Deer et al., 1992). In the XRD analysis, a further study is needed to confirm the type of the interstratifications. However, with reflectance spectroscopy

illite/smectite interstratification was immediately idistiguishable. Comparison of spectrally identifiable clay minerals and XRD analysis results show major similarities with minor inconsistencies.

Mean reflectance spectra for swelling soils and non-swelling were calculated and displayed graphically. They are distinguishable. Remarkably, swelling soils have a lower average reflectance intensity at all wavelengths. This could be attributed to the differences in soil texture, soil moisture, organic matter content, iron oxide content, as they influence overall appearance of soil spectra.

Good correlations that exist between XRD results and laboratory reflectance spectroscopy that can be used to infer engineering parameters (Atterberg limits) of expansive soils. This is supported by the fact that good correlations exist between XRD results and engineering parameters (Atterberg limits) of swelling soils. Hence, laboratory reflectance spectroscopy can be uses as a screening tool for geotechnical investigations.

An ASTER level (3A) scene (date 30 July 2004) that covers most part of the study was used to map swelling and non-swelling soils in the study area. SAM supervised classification method was used. Mean reflectance spectra of swelling and non-swelling soils were used as endmembers for the supervised classification. Furthermore, soil contact/boundaries and classified soil samples were plotted on the map using ArcGIS. This was done to evaluate how well the sample classification will correspond with the ASTER classification. Similarities between image classification and the soil map of the study area were observed. Swelling soils were classified better than the non-swelling soils; only 18.18% of non-swelling soils were correctly classified while 68.75% swelling soils were correctly classified. ASTER image demonstrated potential for mapping expansive soils. This study has confirmed potential for remote sensing techniques as a screening tool for identification of expansive soils and geotechnical investigations.

5.1.1. Scientific contribution

As mentioned before swelling soils pose a significant geological hazard; that causes civil infrastructure damage. Safety of civil infrastructure structures depends on the quality of geotechnical investigations. The success of the study could establish an efficient method to screen geotechnical hazardous soil conditions. It could further enhance appropriate town planning, rural development and risk-management through prevention, mitigation, and adaptation. To the author's knowledge, the multi-technique research reported in this dissertation is one of its kind in South Africa. In particular, research focusing on assessing the capabilities of remote sensing techniques in the identification of expansive soils and geotechnical investigation is limited in South Africa. This project, therefore lays a foundation for further research. The project further demonstrated multidisciplinary approach in the identification and mapping of expansive soil. Hence, this study illustrates a faster, cheaper non-laborious complementary tool that supports traditional methods of mineral identification and geotechnical investigations.

5.2. Limitations and recommendations of the study

5.2.1 Study limitations

Sampling method used was a random sampling method since some areas were inaccessible, some areas are privately owned and the area was built up. The majority of samples were collected in areas with swelling soils; non-swelling soils were insufficiently represented. The number of non-swelling soils as opposed to swelling soils was not enough to split the samples into training and validation set for image classification results.

Limited resources: Basic laboratory tests were conducted and an ASTER image did not over the entire study. Additional test such as clay speciation XRD analysis, particle size distribution and organic matter content enhance the understanding of the soils (clay minerals) which could lead to better interpretation of reflectance spectroscopy results. Spectral reflectance characteristics are a function of factors such as; soil texture, soil moisture, organic matter content, iron oxide content, soil salinity, and surface roughness (Van der Meer, 1999; Jensen, 2007). As mentioned before,

ASTER imagery available for this study did not cover the whole of the study area. This prevented proper comparison between classified ASTER image and the soil map of the study area.

5.2.2. Recommendations

Grid soil sampling: has the ability to provide soil variability at small scale. The grids can be sized such that every soil type in a study area is sufficiently represented. This sampling method is still used for regional geochemical mapping in South Africa (Lombard et al., 1999), and therefore ASTER image mapping capabilities could be better-matched with geochemical maps.

Clay speciation XRD analysis would assist in determining different clay species present within a group. This will improve with the assessment of reflectance spectroscopy's ability to detect different clay minerals. Particle size distribution is an important soil texture property, soil spectral reflectance decreases with increasing particle size (Van der Meer et al., 2012). The presence of organic matter in soil reduces the overall brightness of spectra and may mask out absorption features. If particle size distribution and organic matter content are known than their effect on the soil spectra could be effectively evaluated for better interpretation of the spectra. The ability to better define different soil type spectra could improve the ASTER classification using SAM. Lastly, an ASTER image that covers the entire study area with limited vegetation cover would allow classification accuracy to be performed.

6.0. References

American Association of State Highway and Transportation Officials (AASHTO). (2000). The Materials Book - Standard Specifications for Transportation Materials and Methods of Sampling and Testing. AASHTO

Analytical Imaging and Geophysics, LLC (AIG). (2001) ACORN User's Guide Stand Alone Version, 64pp

Analytical Spectral Device (ASD) (2002). Technical guide, portable spectroradiometers. Boulder, CO: Analytical Spectral Devices.

Al-Rawas, A.A. (1999). The factors controlling the expansive nature of the soils and rocks of northern Oman. *Engineering Geology*, 53, 327-350.

Al-Rawas, A.A., & Goosen, M.F.A. (2006). Expansive Soils: recent advances in characterization and treatment: Leiden, Taylor & Francis, pp. 526

Bedidi, A., & Cervelle, B. (1991). Moisture effects on spectral signature and CIE-colour of laterite soils, In: Proceeding of the 5th International colloquium on physical measurements and signatures in remote sensing, Courchevel, France, 1, 209-212

Bell, F.G. (1983). Engineering properties of Soil and Rocks. London: Butter Worths

Borradaile, G.J. (2003). *Statistics of earth science data: Their Distribution in Time, Space, and Orientation.* Germany: Springer-Verlag Berlin.

Burmister, D.M. (1949). Principles of Techniques of Soil Identification, Proceeding Annual Highway Research Board Meeting, National Research Council, Washington, D.C., 29, 402-433.

Carter, M. & Bentley, S. P. (1991). Correlations of soil properties. London: Pentech Press.

Casagrande, A. (1948). Classification and identification of soils: *Transactions of the American Society of Civil Engineers*, 113, 901-930.

Cawthorn, R.G., Eales, H.V., Walraven, F. Uken, R. and Watkeys, M.K. (2006). The Bushveld Complex. In: Johnson, M. R., Anhaeusser, C. R. and Thomas, R. J. (eds.), The Geology of South Africa. Geological Society of South Africa, Johannesburg/ Council for Geoscience, Pretoria. pp 261-281.

Chabrillant, S., Goetz, A.F.H., Krosley, L. & Olsen, H.W. (2002). Use of hypespectral images in the identification and mapping of expansive soils and the role of spatial resolution. *Remote Sensing of Environment*, 82, 431-445.

Chabrillat, S., Goetz, A. H. (2006): Remote sensing of expansive soils: Use of hyperspectral methodology for clay mapping and hazard assessment. - In: Ali Al-Rawas, A., Goosen, M. F. A. (Eds.), *Expansive Soils: Recent Advances in Characterization and Treatment*, Taylor & Francis, p. 187-209.

Chen, F.H. (1988). Foundation on Expansive Soils. Developments in Geotechnical Engineering, 54. Elsevier Science Publishers.

Chung, F.H., (1974) Quantitative Interpretation of X-ray Diffraction Patterns of Mixtures II. Adiabatic Principle of X-ray Diffraction Analysis of Mixtures. *Journal of Applied Crystallography*, 7, 526-531.

Clark, R.N., King, T.V.V., Klejwa, M. & Swayze, G.A. (1990). High spectral resolution reflactance spectroscopy of minerals. *Journal of Geophysical Research*, 95(B8), 12, 653-12:680

Clark, R.N. (1999). Spectroscopy of Rocks and Minerals, and Principles of Spectroscopy In: Rencz, A. (Ed), Chapter1 in: Manual of Remote Sensing. New York: John Wiley and Sons, Inc.

Clark, R. N., Swayze, G.A., Wise, R., Livo, E., Hoefen, T., Kokaly, R., & Sutley, S.J. (2007). USGS digital spectral library splib06a: U.S. Geological Survey, Digital Data Series 231.

Congalton, R. G. (1991). A review of assessing the accuracy of classification of remotely sensed data. *Remote Sensing of Environment*, 37, 35-46.

Crowely, J.K., & Vergo N. (1999). Visible and Near-Infrared (0.4-2.5µm) reflectance spectra of selected mixed layer clays and related minerals, In: Proceeding of the 6th Thematic Conference on Remote Sensing for Exploration Geology, Applications Technology Economics, 1, 16-19 May 1988, Houston, Texas, 597-606

Das, B. M. (2002). *Principles of Geotechnical Engineering* (5th Ed) Thompson leanings California state University, Sacramento

Day, R.W. (2001). Soil Testing Manual Procedures, Classification, and Sampling Practices. Mcgraw-Hill.

De Senna, J.A., de Souza Filho, C. R., & Angelica, R. S. (2008). Characterization of clays used in manufacturing industry by reflectance spectroscopy: An experiment in the São Simãondall-clay deposit, Brazil. *Applied Clay Science*, 41, 85-98.

Deer, W.A., Howie, R.A., & Zussman, J. (1992). *An introduction to The Rock Forming Minerals.* (2nd Ed) England: Pearson, Prentice Hall.

Department of Public Works (DPW). (2011). Identification of Problematic soils in Southern Africa. Technical Report PW2006/1 for Civil and Structural Engineering.

de Villiers, B. and Mangold, S. (2002) North West Province State of the environment report, The biophysical environment. Geography Dept., Potchefstroom University, Potchefstroom 2. North West Dept. Agriculture, Conservation and Environment, Mafikeng

Diop, S., Heath, L., Ngubelanga, S. and Stapelberg, F (2011). A review on Problem Soils in South Africa. Confidential Report 2011-0062. Pretoria: Council for Geoscience

Erikson, P. G., Altermann, W. and Hartzer, F. J. (2006). The Transvaal Supergroup and its Precursors. In: Johnson, M. R., Anhaeusser, C. R. and Thomas, R. J. (eds.), The Geology of South Africa. Geological Society of South Africa, Johannesburg/ Council for Geoscience, Pretoria. 237-260.

Goetz, A.F.H., Chabrillant, S. & Lu, Z. (2001). Field Reflectance Spectrometry for Detection of Swelling Clays at Construction Sites: *Field Analytical Chemistry and Technology*, 5(3), 143-155.

Good, P. (2005) *Introduction to Statistics Through Resampling Methods* and R/S-PLUS. Wiley.

Gourley, C. S., Newill, D. & Schreiner, H.D. (1993). Expansive soil: TRL's research strategy, in Fookes, P.G., and Parry, R.H.G., eds., First International Symposium on Engineering Characteristics of Arid Soils, Volume PA1301/93:City University, London, July 5-8, Overseas Center, Transport Research Laboratory, Crowthrone, Berkshire, UK., 247-260.

Hauff, P.L. (2000). Manual of Applied Reflectance Spectroscopy with Emphasis on Data Collection and Data Interpretation Using the PIMA-II Spectrometer. User's Manual Arvada, CO, USA, Spectral international Inc.

Hauff, P.L., Kruse, F. A., Madrid, R., Fraser, S. Huntington, J., Jones, M., & Watters, S. (1991). Illite crystallinity-case histories using X-ray diffraction and reflectance

spectroscopy to define ore host environments: in Proceedings, of 8th Thermatic Conference, on Geological Remote Sensing (Denver), 447-458.

Head, K.H. (1994). Manual of Soil Laboratory Testing Volume 2 Permeability, Shear Strength and Compressibility Tests. John Wiley & Sons Inc.

Holtz, R. D., & Kovacs, W. D. (1981). An Introduction to Geotechnical Engineering: Englewood Cliffs. New Jersey: Prentice-Hall, 733.

Horn, G.F.J. & Strydom, J.H. 1998. Clay in The mineral resources of South Africa (M.G.C. Wilson and C.R. Anhaeusser, eds): Handbook, Council for Geoscience, 16, 106 -135.

Hunt, G.R., & Salisbury, J.W. (1970). Visible and near-infrared reflectance spectra of minerals and rocks, I: silicate minerals. *Modern Geology*, 1, 219-288

http://www.icdd.com/translation/productoverview.htm

Jensen, J.R. (2005). *Introductory Digital Image Processing: A Remote Sensing Perspective* (3rd Ed) University of South Carolina: Prentice Hall.

Jensen, J.R. (2007). *Remote Sensing of the Environment: An Earth Perspective* (2nd Ed) University of South Carolina: Prentice Hall.

Kaiser, H.F. (1960). The application of electronic computers to factor analysis. *Educational and Psychological Measurement, 20*, 141-151.

Kalinowski, A. and Oliver, S. (2004). ASTER Mineral Index Processing Manual. Remote Sensing Applications Geoscience Australia.

Kariuki, P.C., Sheperd, K., & van der Meer, F. (2002). Spectroscopy as a tool for studying swelling soils. The Netherlands, ITC

Kariuki, P.C., Van der Meer, F.D., & Siderius, W. S., (2003). Classification of soils based on engineering indices and spectral data. *International Journal of Remote Sensing*, 24 (12), 2567 - 2574.

Kariuki, P.C., Woldai, T. & Van der Meer, F.D. (2004). Effectiveness of spectroscopy to identification of swelling indicator clay minerals. *International Journal of Remote Sensing*, 25(2), 455 - 469.

Kariuki, P.C. (2003). Spectroscopy and Swelling Soils an Integrated Approach.Unpublished PHD thesis. Enschede, The Netherlands, ITC.

King, C., N., Lecomte, V. & Cerdan, O. (2005). The application of Remote Sensing Data to Monitoring and Modelling Soil erosion. Catena, 79-93.

Kruse, F. A., Lefkoff, A. B., Boardman, J. B., Heidebrecht, K. B., Shapiro, A. T., Barloon, P. J. & Goetz A. F. H. (1993). "The Spectral Image Processing System (SIPS) - Interactive Visualization and Analysis of Imaging spectrometer Data." *Remote Sensing of the Environment*, 44, 145 - 163.

Kruse, F. A., & Perry, S. L. (2007). Regional Mineral Mapping By Extending Hyperspectral Signatures Using Multispectral Data: in Proceedings, 2007 IEEE AeroSpace Conference, (peer-reviewed), 3 - 10 March 2007, Big Sky, Montana, On CD-ROM, IEEE Catalog Number 07TH8903C, ISBN: 1-4244-0525-4.

Kruse, F. A. (2004). Comparison of ATREM, ACORN, and FLAASH atmospheric corrections using low-altitude AVIRIS data of Boulder, CO. Summaries of 13th JPL Airborne Geoscience Workshop, Jet Propulsion Lab. Pasadena, CA.

Lambe, T.W., & Whitman, R.V. (1979). *Soil Mechanics*, SI version. New York: John Wiley & Sons, Inc

Lillesand, T.M., Kiefer, R.W., & Chipman, J.W. (2004). *Remote sensing and image interpretation.* (5th Ed) West Sussex: John Wiley & Sons

Lillesand, T. M., Kiefer, R.W., & Chipman, J.W. (2008). *Remote sensing and image interpretation.* (6th Ed.) West Sussex: John Wiley & Sons, Inc

Lombard, M., de Bruin, D., & Elsenbroek, J.H. (1999). High-density regional geochemical mapping of soils and stream sediments in South Africa. *Journal of Geochemical Exploration*, 66, 145-149.

Loubser, M. and Verryn, S. (2008). Combining XRF and XRD analyses and sample preparation to solve mineralogical problems. *South African Journal of Geology*, 111, 229-238.

Low, A.B., & AG. Rebelo (Eds). (1998). Vegetation of South Africa, Lesotho and Swaziland. DEA.T, Pretoria.

Luleva, M. (2007). Identification of Soil Property Variation Using Spectral and Statistical Analyses on Field and ASTER Data A Case Study of Tunisia. Unpublished MSc thesis. The Netherlands, ITC.

Mather, P.M. (2004). *Computer Processing of Remotely Sensed Images* (3rd Ed.) University of Nottingham: John Wiley & Sons.

McKeen, R.G. (1992). A model for predicting expansive behavior of soil, In: Preceding of the 7th International Conference on Expansive Soils, Dallas, TX, 3-5A August 1992, 1-6.

Mitchell, J.K. (1993). *Fundamentals of Soil Behavior*, New York: John Wiley & Son, Inc.

Nelson, J.D., & Miller, D.J. (1992). *Expansive Problems and Practice in Foundations and Pavement Engineering*. New York: John Wiley and Sons, Inc.

Nesse, W. D. (2000). *Introduction to Mineralogy*. New York Oxford: University Press, Inc.

Ninomiya, Y., Fu, B., & Cudahy, T.J. (2005). Detection Lithology with Advanced Spaceborne Thermal Emission and Reflection Radiometer (ASTER) multispectral thermal infrared "radiance-at-sensor" data. *Remote Sensing of Environment*, 99, 127-139.

Okin, G. S. & T. H. (2004). Painter, The effect of Grain Size on Remotely Sensed Spectral Reflectance of Sand Desert Surfaces. *Remote Sensing of Environment*, 89, 272-280.

Olsen, H., Krosley, L., Nelson, K., Chabrillant, S., Goetz, A., & Noe, D. (2000) Mineralogy-Swelling Potential Relationships for Expansive Shales. Advances in Unsaturated Geotechnics, 361-378. doi: 10.1061/40510(287)25

Qui, F. Abdelsalam, M. & Thakkar, P. (2006). Spectral analysis of ASTER data covering part of the Neoproterozoic Allaqi-Heina suture, Southern Egypt. *Journal of African Earth Sciences* 44, 169-180

Rencher, A.C. (2002). *Methods of Multivariate Analysis* (2nd Ed) Brigham Young University: John Wiley & Sons.

Rowan, L. C. & Mars, J.C. (2003). Lithologic mapping in the Mountain Pass, California area using Advanced Spaceborne Thermal Emission and Reflection Radiometer (ASTER) data. *Remote Sensing of Environment*, 84 (3), 350-366.

Shi, B., Jiang, H., Liu, Z. & Fang, H.Y. (2002). Engineering geological characteristics of expansive soils in China. *Engineering Geology*, 67, 63 - 71.

Środoń, J., Drits, V. A., McCarthy, D. K., Hsieh, J.C.C., Eberl, D.D. (2001). Quantitative X-ray diffraction analysis of clay bearing rocks from random preparations. *Clays and Clay Minerals*, 49, 544-528.

Story, M. & Congalton, R. (1986). Accuracy assessment a use's perspective. *Photogrammetric Engineering*. Remote Sensing, 52, 397-399

Syers, J. K., de Vries F. W. T. P., & Nyamudeza, P. (2001). *The Sustainable Management of Vertisols.* New York, CABI Publishing.

Thomas, P. J., Baker, J.C., & Zelazy, L. W. (2000). An Expansive soil index for predicting shrink-swell potential, soil *Society of American Journal*, 64, 268-274.

Van Der Merwe, C. R. (1941) Soil groups and sub-groups of South Africa: Union of South Africa Department of Agriculture. and l% forestry, Chemistry Series No. 165, 316.

Van der Meer, F.D. (1999). Can we map swelling clay with remote sensing? *International Journal of Applied Earth Observation & Geoinformation* (JAG), 1, 27 - 35.

Van der Meer, F.D. (2012). Multi-and Hyperspectral geologic Remote Sensing: A review *International Journal of Applied Earth Observation & Geoinformation,* 14,112 - 128

Vaughan, R.G., Hook, S.J., Calvin, W. M. & Taranik, J.V. (2005). Surface Mineral Mapping at Steamboat Springs, Nevada, USA, with multi-wavelength thermal infrared images. *Remote Sensing of Environment*, 99, 140-158.

Velde, B. (1992). *Introduction to Clay Minerals: chemistry, origins, uses, and environmental significance*. University of California: Chapman & Hall

Williams, A. A. B., Pidgeon, J.T. & Day, P.W. (1985). Problem soils in South Africa-State of the Art. Expansive soils. The Civil Engineer in South Africa, July, 1975, 367-407.

Yamaguchi, Y., Rowan, L. C., Tsu, H. & Kahle, A. B. (1996). Application of ASTER data to geological studies: In Proceedings of the 11th thematic conference on geologic remote sensing; practical solutions for real world problems: 11, I.77-I.86.

Yitagesu, F.A., 2006. Spectroscopy to derive Engineering Parameters of Expansive Soils. Unpublished MSc thesis. The Netherlands, ITC.

Yitagesu, F. A., Van der Meer, F. D. & Van der Werff, H. (2009). Prediction of Volumetric Shrinkage in Expansive Soils (Role of Remote Sensing), Advances in Geoscience and Remote Sensing, Gary Jedlovec (Ed.), ISBN: 978-953-307-005-6

Yitagesu, F.A., Van der Meer, F.D. & Van der Werff, H. (2009). Quantifying engineering parameters of expansive soils from their reflectance spectra. *Engineering Geology*, 105, 151-160

Yitagesu, F.A. (2012). Remote Sensing and Geotechnical Investigations of Expansive soils Unpublished PHD thesis, Enschede, The Netherlands: ITC.

7.0. Appendices

Appendix A. Table 1 Classification of the phyllosilicates and related clay minerals (modified after Horn and Strydom, 1998).

Layer Type	Group	Subgroup	Mineral Species
1:1	Kaolin-Serpentine	Kaolin	Kaolinite
		Serpentine	Berthierine
2:1	Pyrophyllite-talc	Pyrophyllite	Pyrophyllite
		Talc	Talc
	Smectite	Di-smectite	Montmorillonite
		Tri-smectite	Saponite
	Vermiculite	Di-vermiculite	Di-vermiculite
		Tri-vermiculite	Tri-vermiculite
	Mica	Di-mica	Illite, Muscovite
		Tri-mica	Biotite
	Chlorite	Di-chlorite	Sudoite
		Tri-chlorite	Chamosite
	Sepiolite-Palygorskite	Sepiolite	Sepiolite
		Palygorskite	Palygorskite
Variable	Interstratified Mixed-layer	Di-mica-di-smectite	Rectorite
		Tri-chlorite-tri-smectite	Corrensite

Appendix B: XRD diffractogram of sample 2

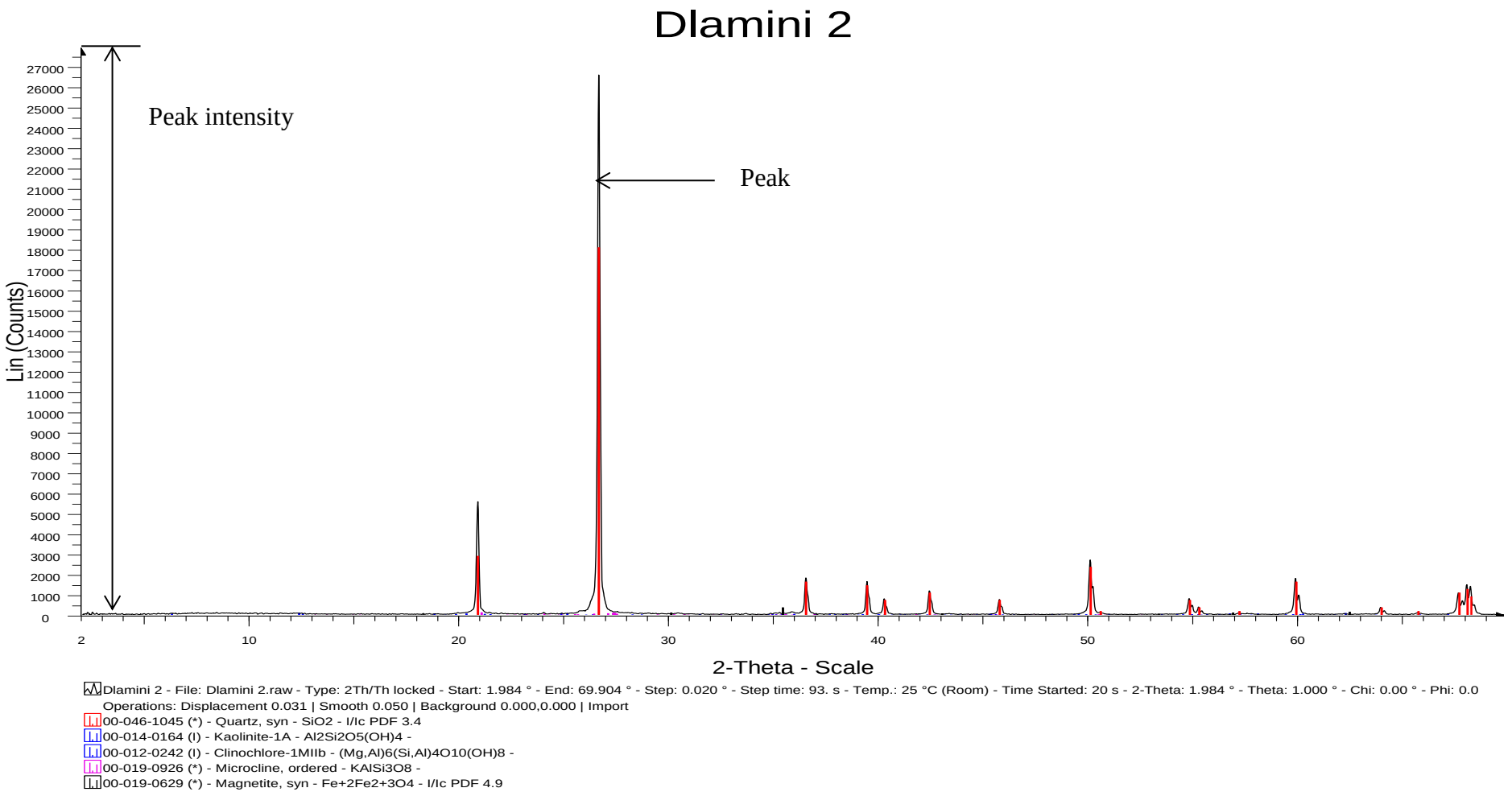

Appendix B: XRD diffractogram of sample 7a

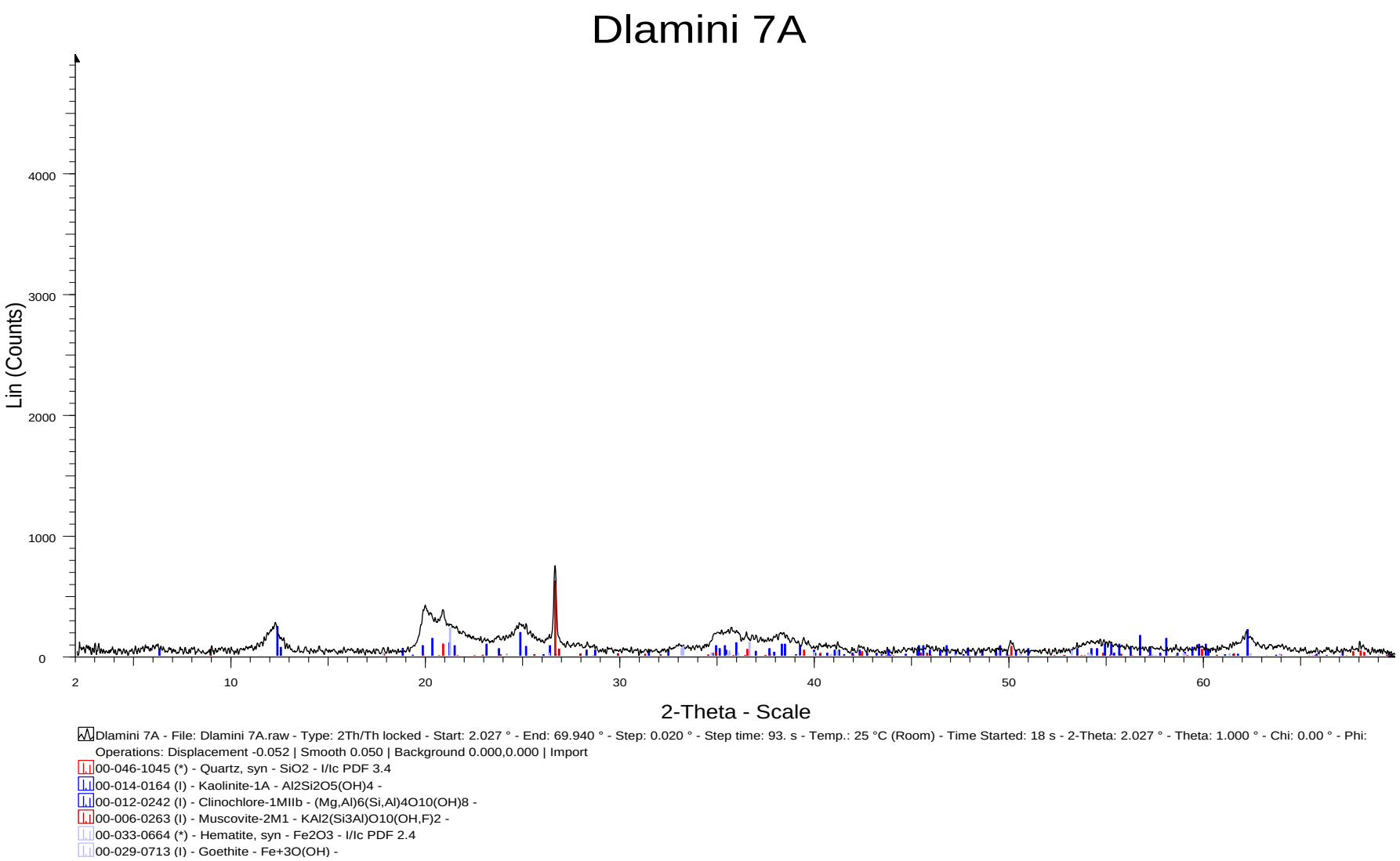

Appendix B: XRD diffractogram of sample 8

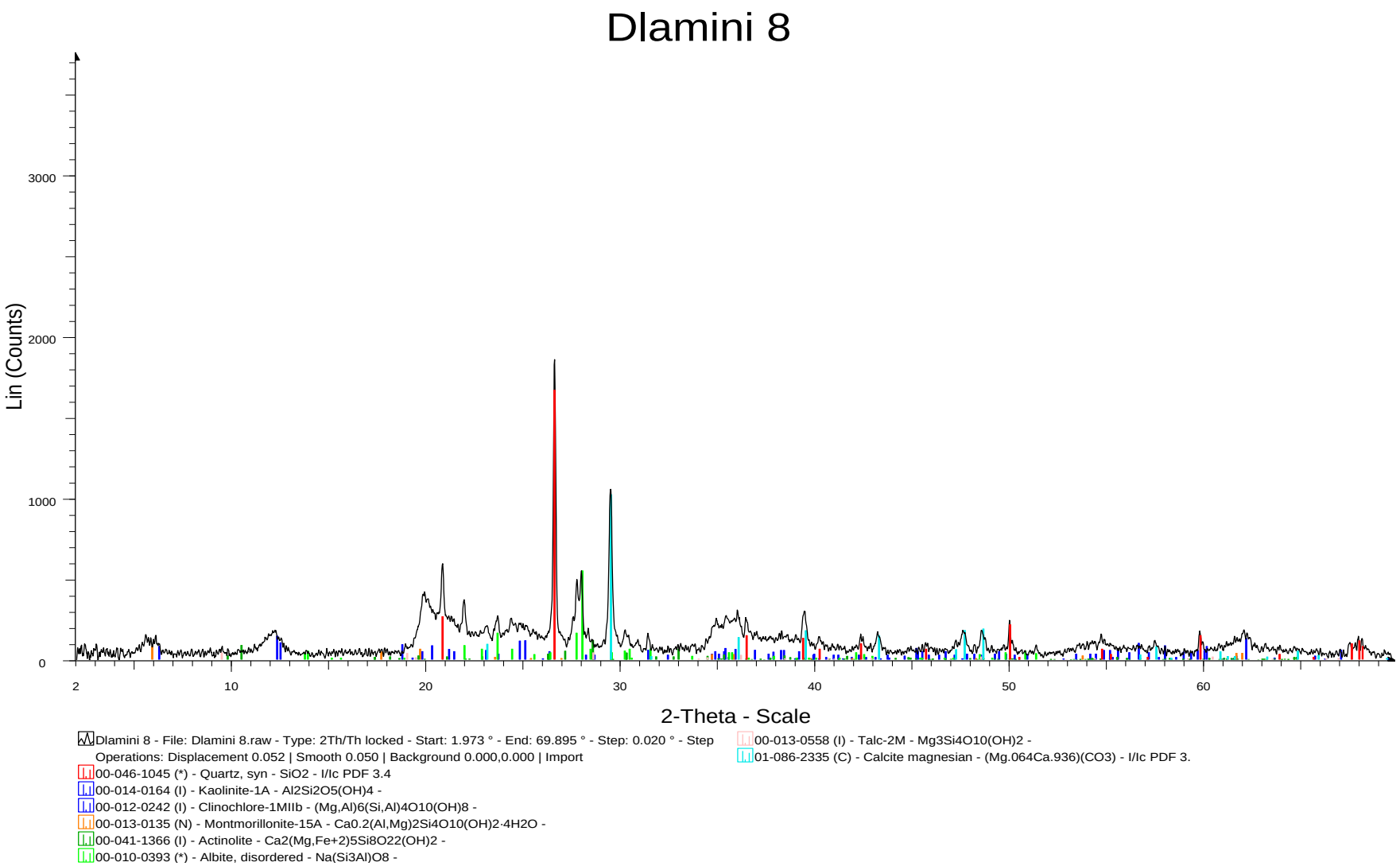

Appendix B: XRD diffractogram of sample 44

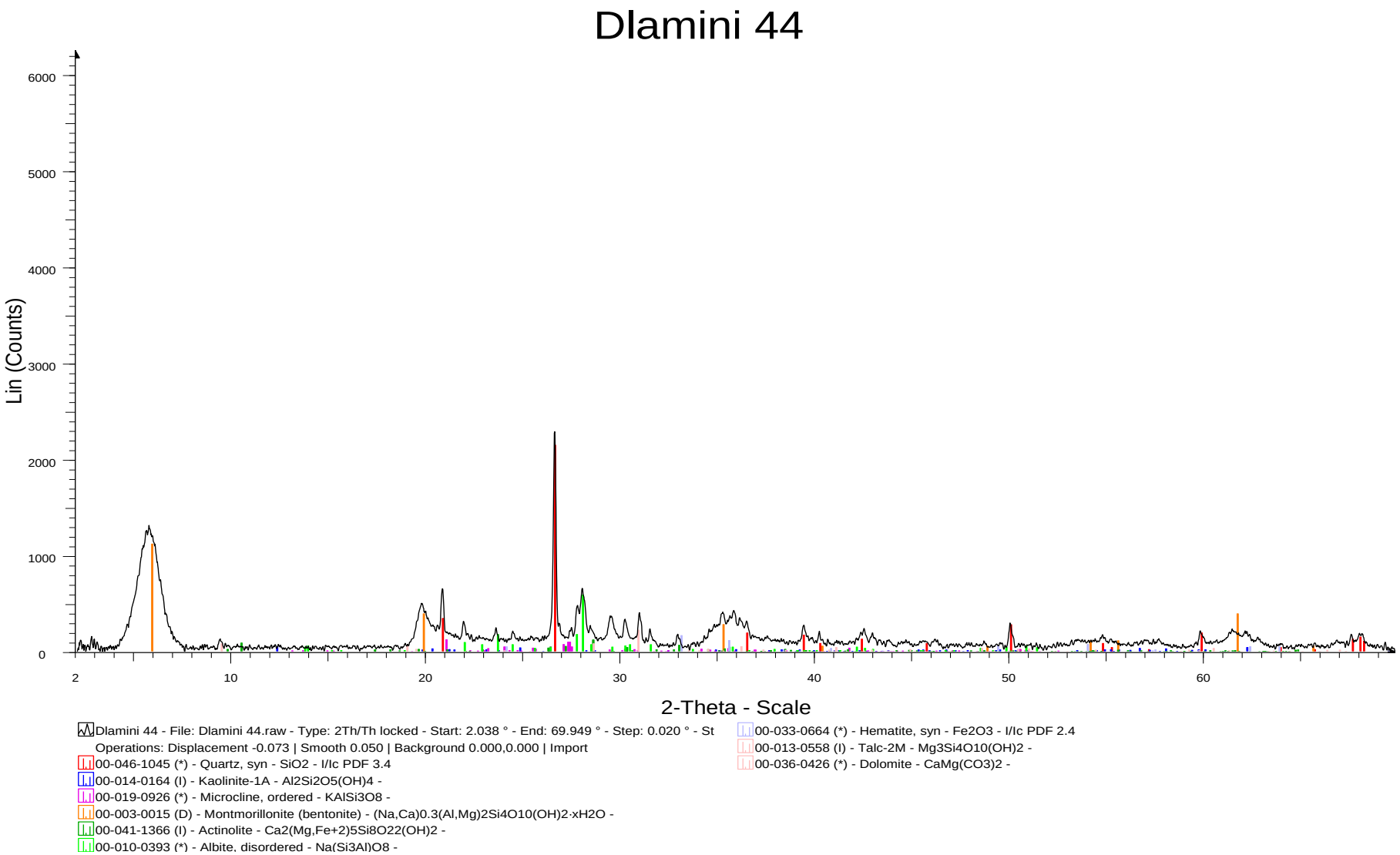

Appendix C: Table 2 XRD results expressed as semi-quantitative estimates of the phase abundances in weight percentages of whole rock analysis (Chung, 1973).

Sample	Hematite / Goethite Fe2O3 / Fe+3O(OH)	Ilmenite Fe+2TiO3	Magnetite Fe+2Fe2+3O4	Magnesioferrite MgFe2+3O4	Calcite CaCO3	Dolomite CaMg(CO3)2	Gypsum CaSO4•2H2O	Amphibole Ca2(Mg,Fe+2)5Si8O22(OH)2	K-Feldspar KAlSi3O8	Plagioclase Na(Si3Al)O8	Quartz SiO2	Mica KAl2(Si3Al)O10(OH,F)2	Talc Mg3Si4O10(OH)2	Palygorskite (Mg,Al)5(Si,Al)8O20(OH)2•8H2O	Chorite (Mg,Al)6(Si,Al)4O10(OH)8	Kaolinite /Chorite	Kaolinite Al2Si2O5(OH)4	Smectite Ca0.2(Al,Mg)2Si4O10(OH)2•4H2O	Interstratification / Mixed-layer clays
1	1	-	-	-	-	-	-	-	2	-	90	3	-	-	-	-	4	-	-
2	-	-	-	-	-	-	-	-	0	1	98	-	-	-	-	-	-	-	-
3	2	-	-	-	-	-	-	-	2	2	80	-	4	-	-	5	-	-	5
4	-	-	-	-	-	-	-	-	-	24	37	-	-	-	-	5	-	35	-
5	5	6	-	-	-	-	-	8	-	16	46	-	-	-	-	-	12	-	7
6	-	-	-	-	-	-	-	37	-	26	6	3	-	-	8	-	-	19	-
7a	7	-	-	-	-	-	-	-	-	-	15	11	-	-	10	-	38	-	19
7b	-	-	-	-	-	-	-	31	-	26	6	3	4	-	-	5	-	26	-
8	-	-	-	-	23	-	-	-	-	14	20	-	5	-	-	12	-	10	15
13	-	-	-	-	-	-	-	5	-	35	24	-	-	-	-	11	-	18	7
14	-	3	-	-	29	-	-	-	-	8	20	-	-	6	-	3	-	31	-
15	5	5	7	-	-	-	-	-	-	24	20	6	-	-	-	10	-	15	8
18	16	13	13	-	-	-	-	-	-	8	35	-	-	-	8	-	-	-	9
19	-	-	-	-	-	-	-	-	-	31	32	-	-	-	-	10	-	11	15
20	17	15	17	-	-	-	-	9	4	9	20	-	-	-	-	10	-	-	-
21	4	4	-	-	-	-	-	-	4	5	27	-	7	-	-	11	-	37	-
23	6	25	-	33	-	-	-	-	-	10	20	-	-	-	-	6	-	-	-

Appendix C: **Table 2 XRD results expressed as semi-quantitative estimates of the phase abundances in weight percentages of whole rock analysis (Chung, 1973).**

Sample	Hematite / Goethite Fe2O3 / Fe+3O(OH)	Ilmenite Fe+2TiO3	Magnetite Fe+2Fe2+3O4	Magnesioferrite MgFe2+3O4	Calcite CaCO3	Dolomite CaMg(CO3)2	Gypsum CaSO4•2H2O	Amphibole Ca2(Mg,Fe+2)5Si8O22(OH)2	K-Feldspar KAlSi3O8	Plagioclase Na(Si3Al)O8	Quartz SiO2	Mica KAl2(Si3Al)O10(OH,F)2	Talc Mg3Si4O10(OH)2	Palygorskite (Mg,Al)5(Si,Al)8O20(OH)2•8H2O	Chorite (Mg,Al)6(Si,Al)4O10(OH)8	Kaolinite /Chorite	Kaolinite Al2Si2O5(OH)4	Smectite Ca0.2(Al,Mg)2Si4O10(OH)2•4H2O	Interstratification / Mixed-layer clays
24	4	12	6	-	-	-	-	-	8	9	49	4	-	-	-	-	6	-	3
25	-	2	-	-	-	-	-	-	15	14	66	2	-	-	-	-	-	-	-
26	3	12	-	-	-	-	-	5	3	7	40	4	-	-	-	6	-	9	11
27	-	-	-	-	-	-	-	2	2	3	87	3	-	-	-	3	-	-	-
28	1	-	-	-	-	-	-	-	-	-	87	2	2	-	-	4	-	-	4
29	-	-	-	-	-	-	-	-	-	-	98	1	-	-	-	1	-	-	-
30	1	1	-	-	-	-	-	-	0	-	94	1	-	-	-	-	3	-	-
31	1	-	-	-	-	-	-	-	1	-	94	1	-	-	-	-	3	-	-
32	-	-	-	-	-	-	-	-	7	3	80	-	-	-	-	4	-	2	4
33	-	-	-	-	-	-	-	4	-	22	32	-	-	-	-	4	-	38	-
34	-	-	-	-	16	-	-	2	-	22	21	-	2	-	-	3	-	34	-
35	2	-	-	-	-	7	-	3	2	9	25	-	3	-	-	3	-	45	-
36	3	-	-	-	-	8	-	-	3	6	28	-	4	9	3	-	-	36	-
37	1	-	-	-	-	-	-	-	1	1	92	-	2	-	-	-	1	-	3
38	1	-	-	-	-	-	-	-	1	-	92	2	2	-	-	-	2	-	-
39	1	-	-	-	-	-	-	-	13	-	64	12	2	-	2	-	7	-	-
40	1	-	-	-	-	-	-	-	11	-	72	9	-	-	-	-	6	-	-

Appendix C: Table 2 XRD results expressed as semi-quantitative estimates of the phase abundances in weight percentages of whole rock analysis (Chung, 1973).

Sample	Hematite / Goethite Fe2O3 / Fe+3O(OH)	Ilmenite Fe+2TiO3	Magnetite Fe+2Fe2+3O4	Magnesioferrite MgFe2+3O4	Calcite CaCO3	Dolomite CaMg(CO3)2	Gypsum CaSO4•2H2O	Amphibole Ca2(Mg,Fe+2)5Si8O22(OH)2	K-Feldspar KAlSi3O8	Plagioclase Na(Si3Al)O8	Quartz SiO2	Mica KAl2(Si3Al)O10(OH,F)2	Talc Mg3Si4O10(OH)2	Palygorskite (Mg,Al)5(Si,Al)8O20(OH)2•8H2O	Chorite (Mg,Al)6(Si,Al)4O10(OH)8	Kaolinite /Chorite	Kaolinite Al2Si2O5(OH)4	Smectite Ca0.2(Al,Mg)2Si4O10(OH)2•4H2O	Interstratification / Mixed-layer clays
41	3	-	-	-	-	4	-	3	-	8	22	-	-	-	-	4	-	56	-
42	-	-	-	-	-	4	-	-	-	22	26	-	-	-	-	-	-	48	-
43	-	13	-	-	-	-	5	-	4	-	41	-	-	-	-	-	-	37	-
44	4	-	-	-	-	7	-	3	3	-	17	-	6	-	-	3	-	58	-
45	1	-	-	-	-	-	-	1	2	-	86	3	-	-	-	-	6	-	-
46	3	-	-	-	-	-	-	-	-	-	79	-	-	-	-	-	12	-	6
47	-	-	-	-	-	2	-	3	3	11	27	-	-	-	-	3	-	51	-
48	12	26	-	-	-	-	-	8	-	12	20	4	-	-	-	7	-	7	4
49	-	5	-	-	-	-	-	4	-	22	44	-	-	-	-	4	-	22	-
50	5	13	-	-	-	-	-	7	3	4	53	6	-	-	-	6	-	-	3
51	2	5	-	-	-	-	-	-	-	5	50	-	-	-	-	7	-	30	-
52	-	-	-	-	-	1	-	-	-	9	72	2	-	-	-	3	-	14	-
53	4	-	-	-	-	-	-	7	-	-	28	-	-	-	-	6	-	56	-
54	4	-	-	-	-	-	-	-	-	32	34	-	-	-	-	8	-	8	14
55	3	-	-	-	-	-	-	4	-	17	27	-	-	-	-	5	-	44	-
66	5	-	-	-	-	-	-	-	-	2	54	18	5	-	-	9	-	-	7
75	-	-	-	-	-	-	-	-	5	1	92	1	-	-	-	1	-	-	-
76	-	-	-	-	-	-	-	-	9	1	85	2	-	-	-	3	-	-	-
77	-	-	-	-	-	-	-	-	7	-	91	-	-	-	-	2	-	-	-

Appendix D: Sample classification into swelling and non-swelling soils based on the presence/absence of smectite or/and interstratification (mixed-layer clays).

Sample	Smectite Ca0.2(Al,Mg)2Si4O10(OH)2•4H2O	Interstratification / Mixed-layer clays	Classification
1	-	-	non-swelling
2	-	-	non-swelling
3	-	5	swelling
4	35	-	swelling
5	-	7	swelling
6	19	-	swelling
7a	-	19	swelling
7b	26	-	swelling
8	10	15	swelling
13	18	7	swelling
14	31	-	swelling
15	15	8	swelling
18	-	9	swelling
19	11	15	swelling
20	-	-	non-swelling
21	37	-	swelling
23	-	-	non-swelling
24	-	3	swelling
25	-	-	non-swelling
26	9	11	swelling
27	-	-	non-swelling
28	-	4	swelling
29	-	-	non-swelling
30	-	-	non-swelling
31	-	-	non-swelling
32	2	4	swelling
33	38	-	swelling
34	34	-	swelling
35	45	-	swelling

Appendix D: Sample classification into swelling and non-swelling soils based on the presence/absence of smectite or/and interstratification (mixed-layer clays).

Sample	Smectite Ca0.2(Al,Mg)2Si4O10(OH)2•4H2O	Interstratification / Mixed-layer clays	Classification
36	36	-	swelling
37	-	3	swelling
38	-	-	non-swelling
39	-	-	non-swelling
40	-	-	non-swelling
41	56	-	swelling
42	48	-	swelling
43	37	-	swelling
44	58	-	swelling
45	-	-	non-swelling
46	-	6	swelling
47	51	-	swelling
48	7	4	swelling
49	22	-	swelling
50	-	3	swelling
51	30	-	swelling
52	14	-	swelling
53	56	-	swelling
54	8	14	swelling
55	44	-	swelling
66	-	7	swelling
75	-	-	non-swelling
76	-	-	non-swelling
77	-	-	non-swelling

Appendix E: Atterberg Limits test results, Liquid limit, Plastic Limit and Linear Shrinkage, Plasticity Index and Potential Expansiveness

Sample	Liquid Limit	Plastic Limit	Plasticity Index	Linear Shrinkage	Potential Expansiveness
1	23	18	5	4	low
2		0	NP	0	none
3	26	13	13	6	medium
4	67	37	30	16	high
5	41	26	15	8	medium
6	37	0	19	10	medium
7a	57	18	25	13	high
7b	-	32	SP	1	low
8	51	28	23	12	high
13	45	25	20	10	high
14	78	45	33	17	high
15	43	21	22	11	high
18	39	19	20	10	high
19	41	20	21	11	high
20	43	26	17	9	medium
21	76	46	30	15	high
23	19	9	10	6	medium
24	33	18	15	7	medium
25		0	NP	0	none
26	59	31	28	14	high
27	22	14	8	4	low
28	26	13	13	6	medium
29	36	28	8	4	low
30	19	11	8	3	low
31	18	12	6	3	low
32	29	15	14	8	medium
33	72	37	37	15	high
34	56	31	25	13	high
35	62	29	33	15	high
36	80	46	34	16	high
37	30	15	15	6	medium
38	24	14	10	4	medium
39	33	23	10	5	medium
40	22	14	8	3	low
41	79	41	38	17	high
42	71	37	34	15	high

Appendix E: Atterberg Limits test results, Liquid limit, Plastic Limit and Linear Shrinkage, Plasticity Index and Potential Expansiveness

Sample	Liquid Limit	Plastic Limit	Plasticity Index	Linear Shrinkage	Potential Expansiveness
43	64	35	29	16	high
44	75	32	43	16	very high
45	24	10	14	6	medium
46	31	17	14	8	medium
47	74	38	36	16	high
48	29	16	13	7	medium
49	51	27	24	12	high
50	24	10	14	6	medium
51	62	26	36	16	high
52	35	16	19	9	medium
53	72	41	31	15	high
54	41	21	20	10	high
55	77	43	34	17	high
66	35	18	17	8	medium
75	23	0	SP	0	low
76		0	NP	0	none
77		0	NP	0	none

Appendix F: XRD hierarchical cluster analysis results

Class	1	2	3
Objects	19	21	8
Sum of weights	19	21	8
Within-class variance	182.77	665.31	672.56
Minimum distance to centroid	4.83	10.32	12.58
Average distance to centroid	11.71	23.66	22.29
Maximum distance to centroid	25.07	44.36	44.14
	1	4	5
	2	6	7a
	3	8	18
	25	13	24
	27	14	26
	28	15	48
	29	19	50
	30	21	66
	31	33	
	32	34	
	37	35	
	38	36	
	39	41	
	40	42	
	46	44	
	52	47	
	75	49	
	76	51	
	77	53	
		54	
		55	

Appendix G: Correlations between minerals (variables) and factors

Minerals	F1	F2	F3	F4	F5	F6	F7
Hematite / Goethite	-0.53	0.65	-0.24	0.05	0.51	0.05	0.02
Ilmenite	-0.34	0.42	0.06	0.27	0.41	0.24	-0.21
Magnetite	-0.28	0.43	-0.08	0.15	0.29	0.25	0.21
Calcite	-0.25	-0.31	0.20	-0.59	-0.13	0.69	-0.19
Dolomite	-0.20	-0.47	-0.68	-0.17	0.21	-0.24	0.15
Amphibole	-0.33	0.01	-0.17	0.46	-0.41	0.01	-0.47
K-Feldspar	0.40	0.10	-0.08	-0.04	0.10	-0.04	-0.23
Plagioclase	-0.59	-0.22	0.30	0.33	-0.29	0.01	0.16
Quartz	0.92	0.18	0.14	0.02	0.12	0.04	0.10
Mica	0.06	0.49	-0.01	-0.27	-0.02	-0.28	-0.48
Talc	-0.15	-0.25	-0.09	-0.48	0.27	-0.25	-0.24
Palygorskite	-0.12	-0.27	-0.36	-0.31	0.05	0.26	0.01
Chorite	-0.35	0.54	-0.46	-0.05	-0.38	0.04	-0.04
Kaolinite /Chorite	-0.56	-0.24	0.70	-0.11	0.22	-0.31	-0.14
Kaolinite	-0.01	0.57	-0.23	-0.35	-0.37	-0.15	0.13
Smectite	-0.48	-0.67	-0.32	0.12	0.01	-0.13	0.04
Mixed Clays	-0.48	0.50	0.37	-0.41	-0.18	-0.18	0.32

Appendix H: **Laboratory measured soil spectra (sample 1-34) showing different absorption feature positions, shapes, and numbers, depth, symmetry, and reflectance intensities.**

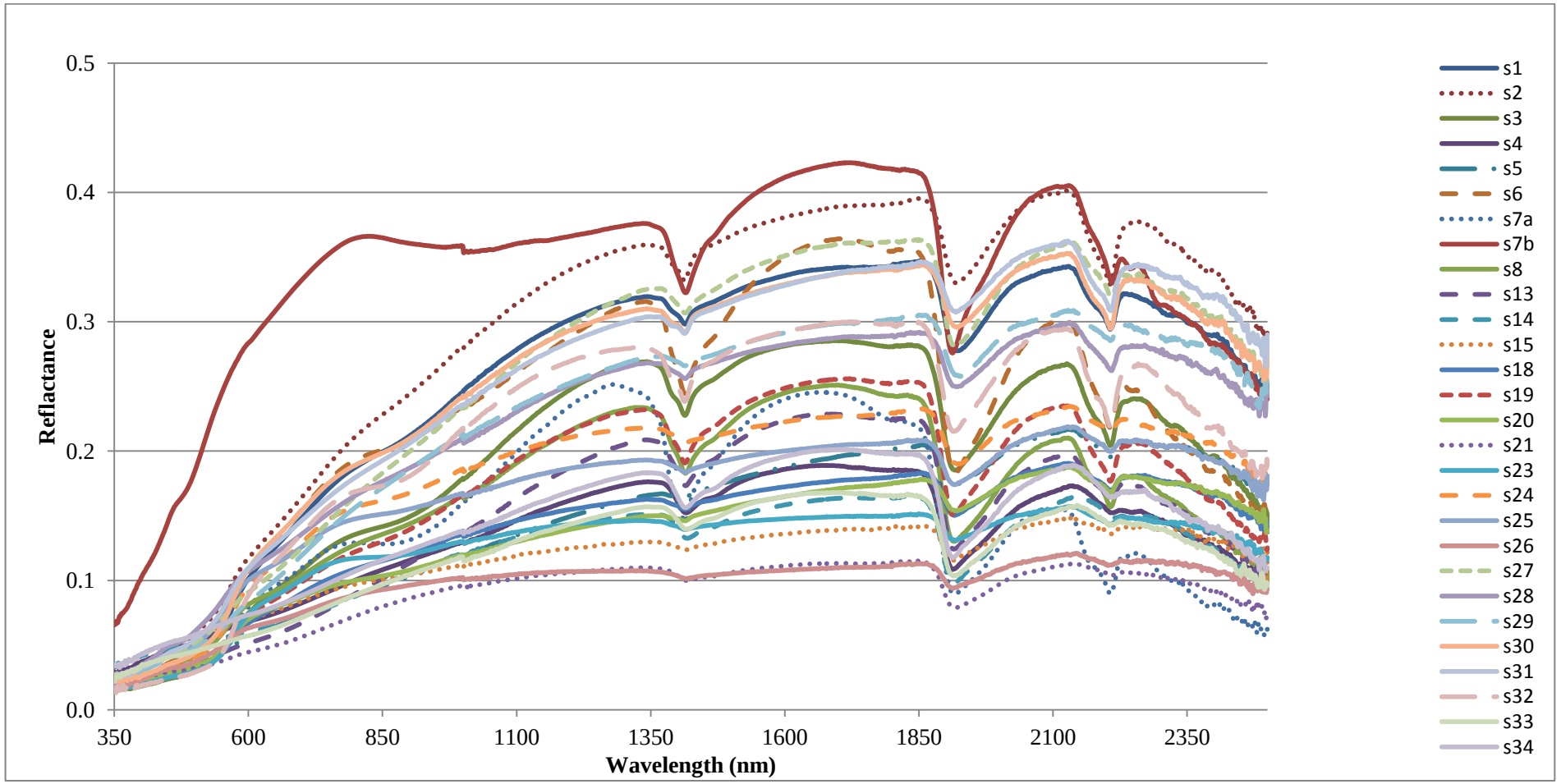

Appendix H: Laboratory measured soil spectra (sample 35-77) showing different absorption feature positions, shapes, and numbers, depth, symmetry, and reflectance intensities.

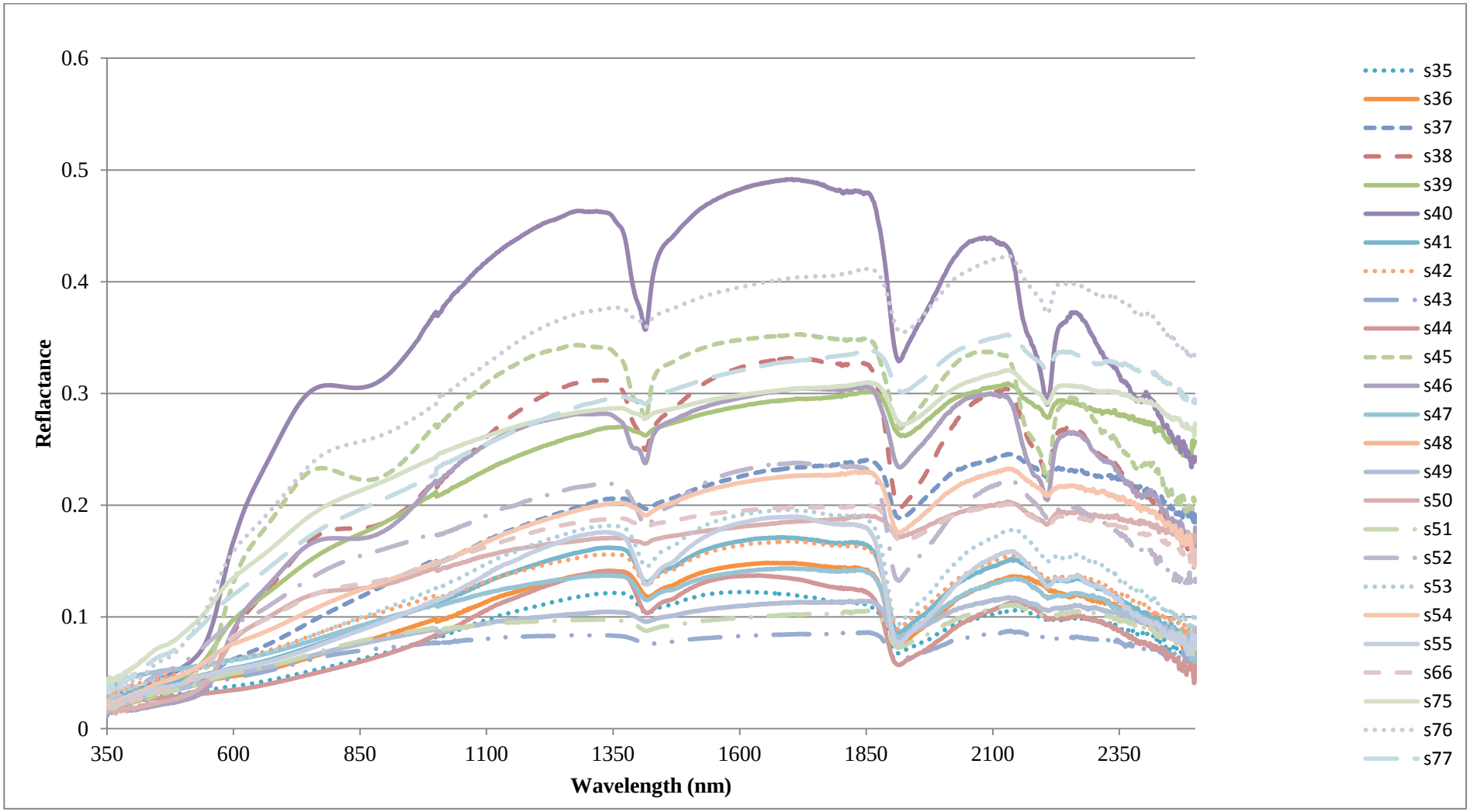

Appendix I: Field Work Report showing sample names, their positions as recorded by a GPS and their colours and texture.

Sample	Latitude	Longitude	Colour Texture
1	-25.7207328	27.78352009	dusky red clayey silt
2	-25.72076172	27.7907245	light brown sandy silt
3	-25.70137203	27.78037629	dark reddish brown silty clay
4	-25.65936335	27.78136318	dark grey clayey silt
5	-25.58540898	27.98570459	dark brown silty clay
6	-25.6025996	27.97797354	pale red spackled light yellowish silty sand
7a	-25.60715323	27.951161	dark reddish brown clay
7b	-25.60715323	27.951161	light olive spackled light grey silty sand
8	-25.60589762	27.93567628	dusky red silty sand
13	-25.60761499	27.92448116	very dark grey sandy silt
14	-25.55652805	27.88335904	dark grey sandy silt clay
15	-25.5643839	27.86170414	dark reddish green sand clay silt
18	-25.56543776	27.83846414	dusky red sandy silt
19	-25.59201937	27.8345549	dark reddish brown clayey silt
20	-25.55590075	27.80776584	dark brown silty clay
21	-25.56030636	27.79507899	very dark grey silty clay
23	-25.54542144	27.85948922	dark reddish brown silty sand
24	-25.53097129	27.82515057	dark reddish brown silty sand
25	-25.52167593	27.80247577	dark yellow silty sand
26	-25.53933148	27.79826352	very dark grey silty clay
27	-25.62752168	27.77862565	very dark brown clayey silt
28	-25.71835762	27.9638005	dark olive silty sandy clay
29	-25.70078982	27.89887008	dark brown silty sand
30	-25.68919715	27.89276898	pale red silty sand
31	-25.69226056	27.88382884	dark reddish brown silty clay
32	-25.66423751	27.79758643	dark red silty clay
33	-25.65571371	27.79774259	dasky blue silty clay
34	-25.65588352	27.81639526	dark grey spackled light grey silty sand
35	-25.66761802	27.83806734	very dark grey silty clay
36	-25.67719409	27.85541628	very dark grey clayey silt
37	-25.68349653	27.86809685	dark reddish brown silty sand
38	-25.70018959	27.84289439	dark red silty sand
39	-25.7262206	27.8374594	light brown silty sand
40	-25.69776328	27.85866209	light reddish orange silty sand

Sample	Latitude	Longitude	Colour Texture
41	-25.66859418	27.8141355	very dark grey silty clay
42	-25.64350194	27.79478461	dark grey spackled light grey silty clay
43	-25.60551298	27.75267209	dark brown silty clay
44	-25.66423391	27.85737086	very dark grey silty clay
45	-25.64982592	27.93597266	light red silty sand
46	-25.62625542	27.95474863	dark reddish brown silty sand
47	-25.62466471	27.89309688	dark grey clayey silt
48	-25.56078957	28.00880159	dark reddish brown silty sand
49	-25.58470407	28.01310218	very dark grey clayey silt sand
50	-25.55472124	27.9890063	dark reddish brown silty sand
51	-25.57116855	27.96849822	very dark grey clayey silt sand
52	-25.62392257	27.93341819	light grey silty sand
53	-25.61104286	27.8966995	dark grey clayey silt sand
54	-25.59112343	27.88338158	dark olive clayey silt sand
55	-25.62069923	27.86081381	very dark grey spackled white clayey silt sand
66	-25.724311	27.962979	reddish brown soils
75	-25.507902	27.761448	light reddish orange silty sand
76	-25.515557	27.885411	reddish brown soils
77	-25.498286	27.93971	reddish brown soils